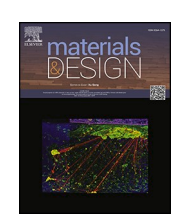


Contents lists available at ScienceDirect

### Materials & Design

journal homepage: www.elsevier.com/locate/matdes





# Generation of novel blue natural biomaterials from fish scales for use in cornea repair and engineering

I. Garzón <sup>a,b</sup>, J. Muñoz-Hurtado <sup>a</sup>, J. Pereira-Martínez <sup>a</sup>, C. González-Gallardo <sup>a,b,c</sup>, A.M. Ionescu <sup>b,d</sup>, J.C. Cardona <sup>b,d</sup>, M. Tejada-Casado <sup>b,d</sup>, M.M. Pérez <sup>b,d</sup>, J. Chato-Astrain <sup>a,b,\*</sup>, M. Alaminos <sup>a,b,\*</sup>

- <sup>a</sup> Tissue Engineering Group, Department of Histology, School of Medicine, University of Granada, Granada, Spain
- <sup>b</sup> Instituto de Investigación Biosanitaria ibs.GRANADA, Granada, Spain
- <sup>c</sup> Division of Ophthalmology, University Hospital Clínico San Cecilio, Granada, Spain
- <sup>d</sup> Laboratory of Biomaterials Optics, Department of Optics, Faculty of Science, University of Granada, Granada, Spain

#### ARTICLEINFO

#### Keywords: Cornea Biomaterials Tissue engineering Blue biomaterials Advanced therapies Fish scales

#### ABSTRACT

Fish scale biomaterials (FSB) were obtained from red scorpionfish (SSC), salmon (SSA), white sea bream (DS) and European carp (CC). Native FSB were preconditioned and cellularized with limbal epithelial cells, and evaluated ex vivo and in vivo. Results showed that preconditioned FSB showed high light transmittance and low reflectance, absorption and scattering coefficients, and proper biomechanical properties. Then, we found that FSB were biocompatible in vivo, and subcutaneous grafting in laboratory animals was not associated with a pathological local or systemic reaction, especially in CC-FSB. After recellularization, FSB supported cell attachment, proliferation and differentiation, with positive expression of limbal epithelial cell markers, and very good optical properties, with the lowest levels of scattering and absorption found in CC-FSB. Intracorneal implant of CC-FSB in laboratory rabbits demonstrated that this biomaterial was also biocompatible to the native cornea, and corneas grafted with CC-FSB had normal expression of corneal epithelium and stromal markers, such as cytokeratin 3, crystallin alpha-A, p63, collagen, proteoglycans and lumican, and devoid of any detectable signs of rejection, inflammation or neovascularization. These findings indicate that CC-FSB potentially meet the criteria for biomaterials used in corneal regeneration, making it a promising candidate for corneal tissue engineering applications.

#### 1. Introduction

The human cornea is an avascular transparent structure composed of three cellular layers: the outer stratified epithelium, the stroma containing keratocytes immersed in a rich extracellular matrix (ECM), and the inner corneal endothelium [1]. An adequate preservation of the cornea structure is crucial for the light to reach the retina [2], and numerous conditions affecting the human cornea can lead to a severe loss of vision and blindness [3]. In addition, several structural pathologies may affect corneal structure and corneal configuration [4], giving rise to structural weakness and dysfunction of the human cornea [5].

In most cases, treatment of these conditions relies on allogeneic corneal transplantation or keratoplasty and, in certain cases, in the surgical implant of a prosthetic material able to reinforce the structure of the corneal stroma [6]. However, these treatments are not devoid of

complications and side effects and, in the case of keratoplasty, there is a strong dependence on the availability of donor corneas [7].

Tissue engineering stands out as a promising and innovative alternative to address the shortage of corneal grafts and offer new therapeutic approaches for complex corneal conditions [8]. In fact, several bioengineered corneal tissues have been described to the date, with some of them showing promising results in cases of severe and extensive corneal damage [9]. In addition, several biomaterials have been developed for treating conditions that compromise corneal integrity. Biomaterials intended for corneal tissue engineering must meet several essential criteria, including high biocompatibility, structural integrity, suitable mechanical strength, and optical transparency, among others [10]. While numerous biomaterials have been proposed for the clinical management of corneal conditions, including materials of natural origin such as fibrin, alginate, collagen [11] and synthetic materials such as

<sup>\*</sup> Corresponding authors at: Tissue Engineering Group, Department of Histology, School of Medicine, University of Granada, Granada, Spain. E-mail addresses: jchato@ugr.es (J. Chato-Astrain), malaminos@ugr.es (M. Alaminos).

methacrylate and polyethylene glycol-polycaprolactone [12], all these biomaterials are associated to important limitations such as deformability, mechanical weakness, and low integration in the native tissues [13]. For these reasons, development of novel fully biocompatible biomaterials with potential utility in corneal repair is in need [14,15], and interesting materials based on hyaluronic acid [15,16] and nanoparticles and nanofibers [14,17] have been described to date.

Blue biomaterials are natural products obtained by sustainable byproducts sources that can be recovered to minimize waste and contamination, thus generating novel value-added products [18]. A promising source of natural blue biomaterials with potential usefulness in corneal repair and engineering is the fishery and aquaculture industry [19,20]. In fact, this industry accounts for a very important economic activity in numerous countries worldwide, and the high amounts of natural by-products generated by this activity are innumerable. Among others, fish scales are dermal-origin structures present in most species of bony fishes that play an important protective role of the body structures of these animals [21]. Interestingly, fish scales are normally transparent and mechanically resistant, and fulfill most requirements for use in cell culture and tissue engineering [22]. For these reasons, the use of fish scale biomaterials (FSB) has been preliminarily described in several scenarios [23], although none of these scaffolds was fully characterized. In general, most types of fish scales consist of a complex mixture of organic compounds, especially type-I collagen, and inorganic compounds forming a mineralized matrix similar to hydroxyapatite [24]. Interestingly, the plywood structure and the fine alignment of the collagen fibrils within the fish scale are able to partially reproduce the defined structure of collagen within the human cornea, offering an additional advantage for the use of FSB [22]. Although some reports suggest the usefulness of FSB as natural biomaterials in cornea repair and engineering [25], only three species of fish have been evaluated to the date, and nearly 80 % of these reports were focused on the use of tilapia (Oreochromis niloticus) fish scales [25,26]. In addition, characterization is typically performed partially, and no reports were able to fully characterize and evaluate these products ex vivo and in vivo.

In this study, we analyzed four types of FSB obtained from four common species of fish available in all European fish markets as putative biomaterials for use in corneal repair and engineering. These FSB were evaluated *ex vivo* to determine their main physical properties (i.e., biomechanical and optical properties), their histological structure and composition and their potential to sustain corneal epithelial cell attachment and differentiation. In addition, FSB were implanted in laboratory rats to determine their biocompatibility and were implanted in the cornea of laboratory rabbits to evaluate their functionality and potential usefulness in corneal surgery.

#### 2. Materials and methods

#### 2.1. Obtaining the fish scale biomaterials (FSB) used in the present work

To obtain the fish scale biomaterials (FSB), four species of commercially available fish were purchased at a local fish market, including the red scorpionfish (*Scorpaena scrofa* –SSC-), salmon (*Salmo salar* –SSA-), white sea bream (*Diplodus sargus* –DS-) and the European carp (*Cyprinus carpio* –CC-). 200 scales were obtained from each species using surgical forceps. These scales were rinsed in distilled water and phosphate-buffered saline (PBS) (Merck, Darmstadt, Germany) and were used as native FSB (N-FSB). Preconditioned FSB (P-FSB) were prepared by incubating the scales in Morse solution composed of a 1:1 mixture of 20 % sodium citrate and 50 % formic acid (Merck) in water for 24 h at room temperature with slight agitation, followed by several rinses in sterile distilled water. All these procedures were carried out using sterile materials and reagents, and P-FSB were briefly immersed in 70 % ethanol for 5 s, and then rinsed three times in distilled water for sterilization.

Cellularized FSB (C-FSB) were obtained by culturing SIRC rabbit

limbal epithelial cells generated by the Statens Seruminstitut Rabbit Cornea (ATCC, Manassas, VA, USA) on the surface of each P-FSB. In brief, cells were enzymatically dissociated from the culture flask with trypsin-EDTA, and placed on the surface of each P-FSB (200,000 cells/cm $^2$  of biomaterial). To promote cell adhesion, P-FSB were previously incubated for 24 h in fetal bovine serum (Merck). These C-FSB were maintained in a cell incubator at 37  $^{\circ}\text{C}$  with 5 % carbon dioxide under standard culture conditions using a culture medium containing Eagle Medium Modified by Dulbecco (DMEM) (Merck), 10 % bovine serum (Merck) and 1 % of a cell culture solution of antibiotic-antimycotics (Invitrogen-Thermo Fisher Scientific, Waltham, MA, USA). C-FSB were kept in culture for 4 days.

#### 2.2. Characterization of the optical properties of FSB

First, the gross translucency of each type of FSB (N-FSB, P-FSB, and C-FSB) was evaluated by placing each biomaterial on a white surface in which a black letter had been printed. Human native corneas were used as controls (CTR). Then, the optical properties of these biomaterials were analyzed using the IAD method (Inverse Adding-doubling), as previously reported [27]. For this, samples were placed in a customized double-integrating sphere, and the diffuse transmittance and reflectance were quantified in the visible wavelength (400-780 nm) using a white light emitter (240-1100 nm, Thorlbas, Germany) that was linked to the sphere by optic fibers (M92L01,  $\Phi=200~\mu m,\,0.22NA$ ). In addition, the absorption and the reduced scattering coefficients of each material were quantified from the diffuse reflectance and transmittance results by applying the IAD algorithm found at https://omlc.org/software/iad/. Then, the values of the diffuse reflectance and transmittance were calculated and compared with the values previously measured experimentally, assuming a g value of 0.98. Iterations were performed until the experimental data corresponded with the calculated values, with a tolerance difference of 0.01 %. We considered that the refractive index was n = 1.589, as previously reported for this type of material [28]. Three samples of each type of FSB were analyzed (n = 3).

#### 2.3. Characterization of the biomechanical properties of FSB

The main biomechanical properties of FSB were analyzed under tensile strain using a 3345-K3327 Instron (Norwood, MA, USA) electromechanical material testing machine with a BlueHill 3 Material Testing software, as previously reported [29]. FSB samples were fixed to the clamps of the analysis device, leaving a gap of 0.5 cm between the two clamps. These analyses were performed applying a strain at 5 mm/min at room temperature, up to the point of material fracture. In all cases, we determined the modulus of Young, the strain at fracture and the traction deformation by analyzing the linear region of the stress—strain curve. For the Young's modulus, we measured the tangent modulus of the linear region of the curve, whereas the strain at fracture was identified at the point where the material failed, and the traction deformation was defined as the percentage elongation the FSB achieved before rupture. Results were obtained using a 100 N Instron load cells. We analyzed 8 different samples of each FSB (n = 8).

#### 2.4. In vivo evaluation of FSB

First, biocompatibility was evaluated by subcutaneously grafting each P-FSB in laboratory rats. In brief, animals were subjected to general anesthesia, and five subcutaneous pouches were created on the back of each animal, close to the origin of each member and the tail. Then, a P-FSB was inserted within each pouch, and fixed to the surrounding tissues using suture material, and the skin wound was sutured using the same material. Three animals were used per study group, and each animal always received the same type of P-FSB in all pouches (n = 3, with 5P-FSB samples per animal). After 30 days, animals were deeply anesthetized and euthanatized, and whole blood samples were obtained for

analysis of hematological and biochemical markers using an automatic analyzer Sysmex KX-21 N and Cobas c311 (Roche, Basel, Switzerland). In addition, the grafting area was surgically excised for histological analysis.

Then, functionality of selected FSB showing good results in the previous analyses was determined by implanting these biomaterials in the cornea of laboratory rabbits. For this, animals were anesthetized, and a intracorneal pocket was created in the corneal stroma of each animal using a crescent ophthalmic knife under microscopical vision. FSB were then placed within the intrastromal pouch and the wound was repaired using 10/0 nylon suture stitches. This surgical intervention was performed in the right eye of 4 laboratory rabbits (n=4), whereas the left eye was left untouched and served as control. These animals were monitored for 3 months, and clinical images were obtained with anterior pole optical coherence tomography (OCT) and using a slit lamp. Then, corneas were excised for histological analysis.

#### 2.5. Histology, histochemistry and immunohistochemistry analysis of FSB

For light microscopy analysis, the specimens were fixed in neutral formalin, subjected to ethanol dehydration, cleared with xylene and embedded in paraffin (all these products were purchased to Panreac AppliChem (Barcelona, Spain) following routine histological methods. Tissue sections with a thickness of 4 µm were obtained with a microtome, and sections were dewaxed and rehydrated using xylene, ethanol and water. To identify cell nuclei in a specific sample, a mounting medium with DAPI (4',6-diamidino-2-phenylindole) (Vector Laboratories, Burlingame, CA, USA) was applied on the surface of tissue sections, and a coverslip was then applied. Samples were examined and photographed using a Nikon Eclipse i90 microscope with fluorescent light. For histological analysis of general structure, sections were stained with hematoxylin and eosin (HE) by incubation in hematoxylin for 3 min, water differentiation for 5 min and eosin staining for 1 min (Panreac Appli-Chem). Samples were covered with coverslipped using a mounting medium (Vector Laboratories) and a Pannoramic Flash Desk DW histological scanner (3DHISTECH, Hungary) was used to scan the slides and obtain the histological images.

Identification of extracellular matrix (ECM) components was performed by histochemistry following previously described methods [30]. To identify calcium mineralization deposits, we used alizarin red S (AR). For this, tissue sections were immersed for 2.5 min in a 1 % aqueous solution of alizarin red (Merck) at pH 4.2, and dehydrated using a 50 % xylene-50 % acetone solution. In order to detect collagen fibers, samples were stained with picrosirius red (PSR). For this, tissue sections were incubated in a saturated aqueous solution of picric acid containing 0.2 % (w/v) of sirius red F3B powder (Merck) for 45 min, followed by brief counterstaining with Harris' hematoxylin for 1 min. To reveal the presence of acid proteoglycans, tissue sections were incubated in an alcian blue solution for 30 min, followed by nuclear fast red counterstaining for 1 min. Samples were coverslipped using mounting medium (Vector Laboratories) and scanned with a Pannoramic Flash Desk DW histological scanner (3DHISTECH, Hungary).

The specific detection of cell and tissue components was carried out by indirect immunohistochemistry, following routine laboratory analysis methods. In short, samples were treated with a buffer solution with 50 % horse serum and 50 % casein (Vector Laboratories), and incubated with a specific primary antibody for 2 h at room temperature. After washing in PBS, a pre-diluted secondary antibody was applied (Vector Laboratories), and sections were treated with a DAB (diaminobenzidine) substrate kit (Vector Laboratories). Nuclear counterstaining was then performed with Harris' hematoxylin (Invitrogen-Thermo Fisher Scientific) for 4 min. Tissue sections were coverslipped scanned. Specific conditions applied to each immunohistochemical analysis are shown in Supplementary Table S1.

Evaluation of the histochemical and immunohistochemical analysis of AE1/AE3, CK3, CRY- $\alpha$ A,  $\Delta$ Np63, TJP1, KI67, CD34, LUM, PSR and AB

was performed by semiquantitatively scoring the positive signal as previously reported [31]. In brief, the signal was assessed as negative (-), slightly positive (+/-), positive (+), very positive (++), or strongly positive (+++).

To characterize the surface of samples using scanning electron microscopy (SEM), specimens were fixed for 24 h in 0.1 M phosphate buffer (pH 7.2) containing 2.5 % glutaraldehyde at 4 °C, washed twice in 0.1 M PBS, and dehydrated with acetone (30 %, 50 %, 70 %, 95 %, 100 %) (all these products, from Panreac AppliChem). Complete dehydration was then achieved using the critical point method, and samples were gold-coated and analyzed using a FEI Quanta 200 scanning electron microscope (FEI, Eindhoven, The Netherlands). SEM images were used to determine surface roughness in native and preconditioned FBS using the ImageJ program, as previously reported [32]. In brief, a square figure of  $50\times50~\mu m$  was selected in each image, and the plot profile option of the software was used to obtain a list of plot values corresponding to each sample expressed as surface plot arbitrary units (U) ranging from 0 U (smooth surface) to 255 U (maximum roughness).

#### 2.6. Statistical analysis

The biomechanical parameters obtained for each sample, and the hematological and biochemical parameters obtained in blood of the animals were first analyzed for normality. For this, we first analyzed each variable with the Shapiro-Wilk test, and we found that most variables did not meet the assumptions for parametric analysis. In consequence, non-parametric statistical tests were employed to compare the results obtained in different study groups. For the overall comparison of several samples at the same time (for example, a comparison among the four types of N-FBS, i.e. N-SSC, N-SSA, N-DS and N-CC), we used the test of Kruskal-Wallis. For the pairwise comparison of two specific groups (for example, a comparison between N-SSC vs. N-SSA), we used the test of Mann-Whitney. For the optical parameters, we also determined how similar the spectral behavior of the optical properties were using the Root Mean Square Error (RMSE) and the Goodness-of-Fit coefficient (GFC) metrics, as previously reported [33,34]. The absolute differences that can be detected between two spectral curves can be analyzed by the RMSE, which focuses on the magnitude of this difference, which depends on scale factors. A RMSE value of 0.02 or less indicates a good agreement in spectral quality between the compared metrics. In turn, a GFC equal to 1 indicates a perfect spectral match between the compared curves, whereas GFC between 0.9990 and 0.9999 indicate that a very good and an excellent spectral match exists, respectively. As multiple tests were carried out in the present work, a Bonferroni-corrected p value below 0.001 was considered as statistically significant. Statistical tests were conducted using RealStatistics software (version 7.2) (Dr. Charles Zaiontz, Purdue University, IN, USA), available at https://www. real-statistics.com/.

#### 3. Results

## 3.1. Histological evaluation of native (N-FSB) and preconditioned fish scale biomaterials (P-FSB)

Histological analysis of the N-FSB evaluated in this study revealed the presence of a homogenous dense material, although differences were detected among the four types of N-FSB (Fig. 1). First, our analysis using HE staining revealed that N-FSB consisted in a thin layer of dense material containing some cells, especially at the apical region. Scales corresponding to the SSC and DS group were very thin, whereas SSA and CC had higher thickness. In addition, the internal structure of most types of N-FSB, especially CC, was heterogeneous, and showed numerous layers of material. Analysis of P-FSB using HE staining showed that all P-FSB kept their original structure after preconditioning, without any relevant artifacts generated by this process.

In order to identify the cell population of each FSB, we also used

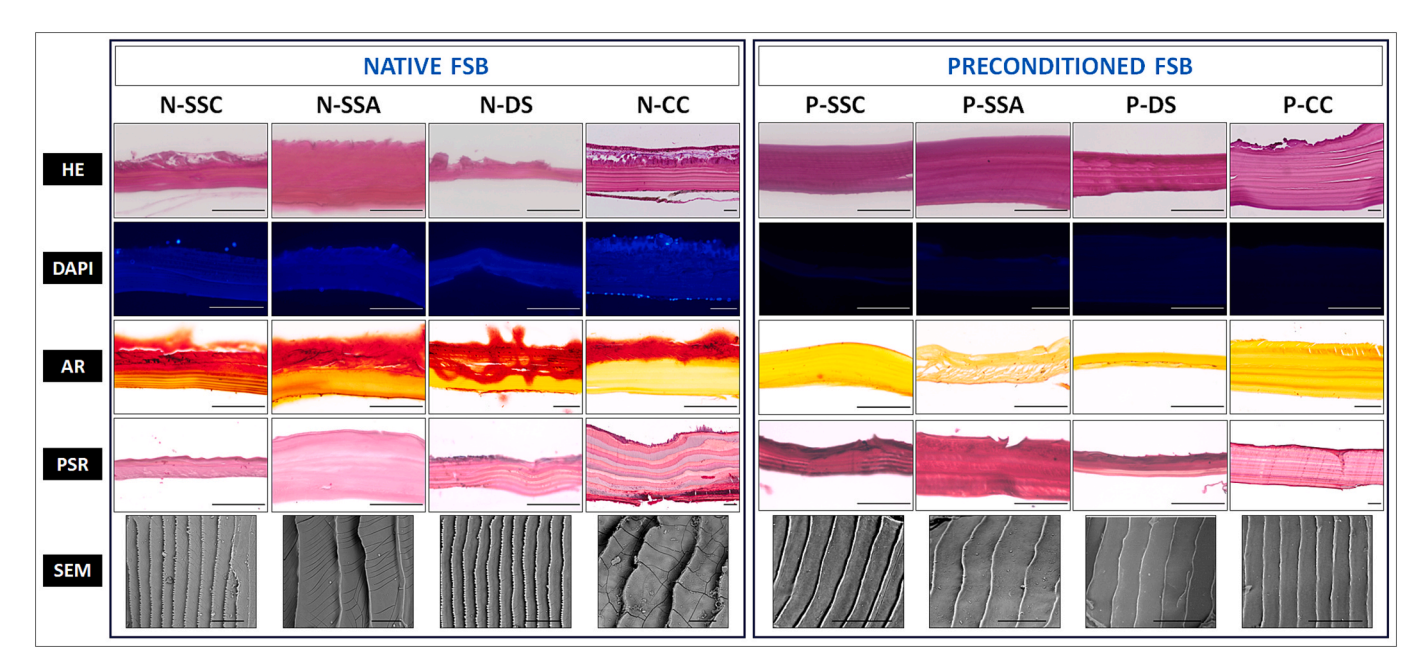


**Fig. 1.** Histological analysis of native and preconditioned fish scale biomaterials (FSB). HE: analysis using hematoxylin and eosin (HE); DAPI: identification of cell nuclei using 4′,6-diamidino-2-phenylindole (DAPI) staining; AR: alizarin red histochemistry; PSR: picrosirius red histochemistry; SEM: scanning electron microscopy analysis. SSC: *Scorpaena scrofa* (red scorpionfish); SSA: *Salmo salar* (salmon); DS: *Diplodus sargus* (white sea bream); CC: *Cyprinus carpio* (European carp). Scale bars: 100 μm for HE, DAPI, AR and PSR and 50 μm for SEM. (For interpretation of the references to colour in this figure legend, the reader is referred to the web version of this article.)

DAPI staining (Fig. 1). Results showed that native SSC and CC contained abundant cells at the apical region, with CC also containing a cell layer at the basal region of the scale. Cells were less abundant in SSA and DS. When FSB were subjected to preconditioning, we found that DAPI staining was negative in all P-FSB, suggesting that all cells in the scales were properly removed by the preconditioning process.

Then, we evaluated the presence of calcium deposits using AR histochemistry. As shown in Fig. 1, results showed that all N-FSB showed a strong positive histochemical signal, which confirms the presence of calcium deposits, especially at the apical region. In contrast, our analysis of P-FSB using AR showed that preconditioning was able to remove calcium deposits from all samples, and all P-FSB showed very low signal for this histological technique.

On the other hand, we examined the presence of collagen fibers using PSR histochemistry (Fig. 1). In N-FSB, our results showed that all scales consisted of a series of layers of material showing positive PSR signal, suggesting that collagen fibers were present in all types of N-FSB. Then, the analysis of collagen fibers in P-FSB showed that collagen fibers were present in the four types of samples, and preconditioning was not associated to a decrease in the staining signal found in P-FSB.

Finally, we evaluated the surface of each FSB using SE. As shown in Fig. 1, the surface of all scales consisted of several layers of parallel, overlapping lamellae. The FSB showing the highest number of lamellae were SSC and DS, whereas SSA and CC apparently contained fewer, but larger lamellae. In addition, the edge of the lamellae in native SSC and DS was covered with small electrodense spike-like spicules, whereas SSA and CC were devoid of these structures. After preconditioning, we found that the surface of all scales was properly preserved, and all scales showed the typical layers of parallel overlapping lamellae, with no evident alterations of the structure of this surface. However, our results showed that preconditioning was associated with a complete elimination of the electrodense spike-like spicules found at the edge of the lamellae of SSC and DS. Furthermore, the analysis of surface roughness revealed that preconditioning was associated to a trend to reduce this parameter in the SSC (132.85  $\pm$  7.4 U in N-SSC vs. 104.58  $\pm$  5.84 U in P-SSC) and CC groups (117.33  $\pm$  3.28 U vs. 109.36  $\pm$  1.54 U), but not in the SSA and DS groups, although differences were not statistically

significant (p = 0.0285 for SSC and CC and p > 0.05 for SSA and DS).

#### 3.2. Analysis of the physical properties of N-FSB and P-FSB

Analysis of the biomechanical properties of FSB revealed significant differences among the groups (Fig. 2 and Table 1). For the Young's modulus, global differences among the four types of N-FSB and among the four types of P-FSB were detected (p = 0.0001 for the test of Kruskal-Wallis for N-FSB and p < 0.0001 for P-FSB). For the native FSB, the maximum values of Young's modulus were found in N-CC, and the lowest values, in N-SSA, with differences being statistically significant (p = 0.0002 for the Mann-Whitney test). Differences among native samples were not significant for the strain at fracture and for the traction deformation. When the FSB were preconditioned, we found significant differences among the four types of P-FSB for the Young's modulus (p < 0.0001 for the test of Kruskal-Wallis), with the highest values found in P-DS and P-CC, with differences with P-SSC and P-SSA being statistically significant (Table 1). Interestingly, a significant decrease in the Young's modulus was found in P-SSC, compared with N-SSC (p = 0.0002 for the Mann-Whitney test), along with a significant decrease in P-SSA as compared to N-SSA (p = 0.0003) and in P-CC as compared to N-CC (p =0.0002). In the case of the strain at fracture, significant differences among the four P-FSB were detected (p < 0.0001 for the test of Kruskal-Wallis), with the highest values found in P-CC, which showed significant differences with the other types of P-FSB (Table 1). Preconditioning was associated with a significant reduction of this biomechanical parameter in SSA (p = 0.0003) and an increase in CC samples (p = 0.0006). For the traction deformation, differences among samples were not statistically significant.

On the other hand, the analysis of the optical behavior of N-FSB and P-FSB (Fig. 2 and Tables 1 and 2) revealed that all these materials were transparent. First, our gross analysis of translucency showed that all the fish scales used in the present work were apparently transparent and allowed the incoming light to go through these materials, and preconditioning resulted in an apparently slight increase in the translucency of all samples. Then, assessment of the optical behavior of N-FSB and P-FSB (Fig. 2 and Table 1) confirmed that these biomaterials have

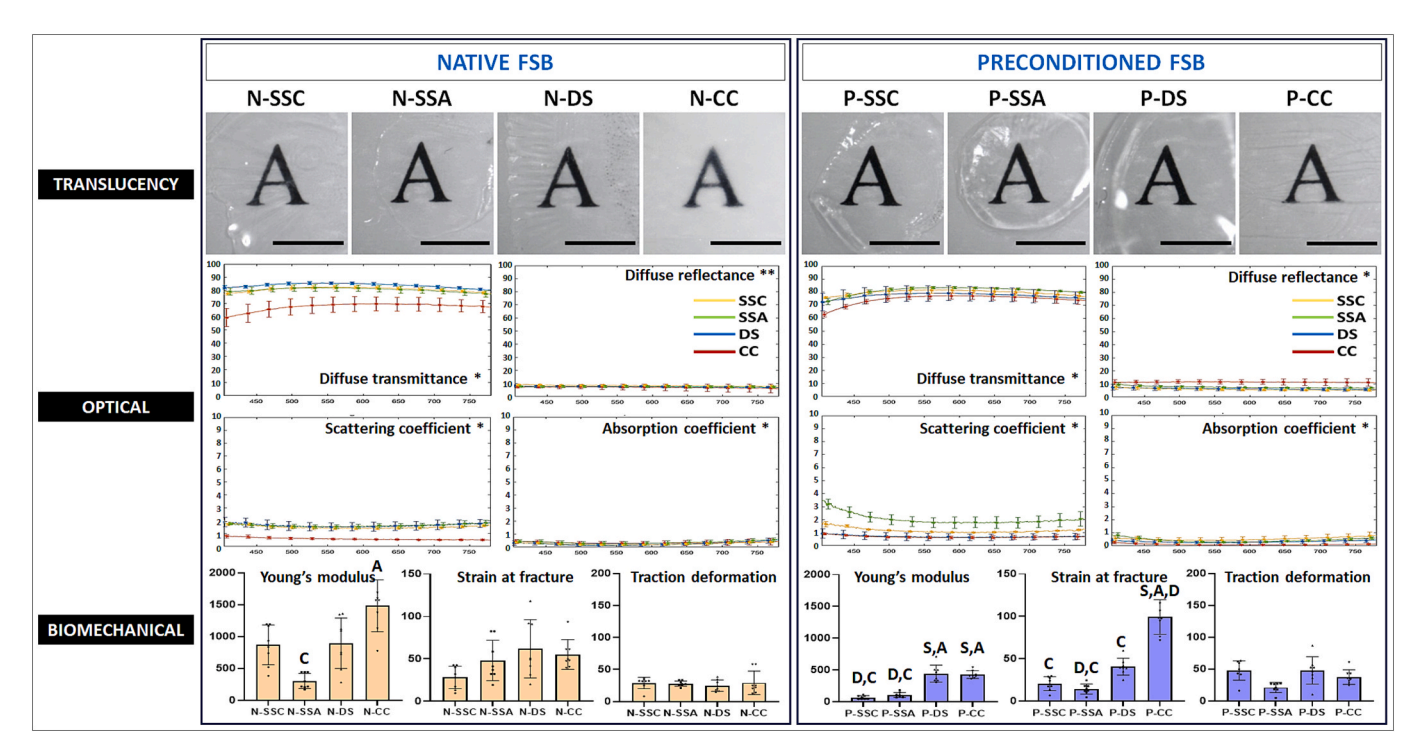


Fig. 2. Evaluation of the physical properties (optical and biomechanical) of native and preconditioned fish scale biomaterials (FSB). Translucency: gross transparency analysis of FSB deposited on a black printed letter; Optical: Results of the analysis of the diffuse transmittance, diffuse reflectance, scattering and absorption coefficient optical properties of FSB; Biomechanical: Analysis of biomechanical properties of FSB as determined by the strain at fracture, Young's modulus and traction deformation. Results correspond to mean values, whereas error bars represent standard deviations. SSC: Scorpaena scrofa (red scorpionfish); SSA: Salmo salar (salmon); DS: Diplodus sargus (white sea bream); CC: Cyprinus carpio (European carp). Scale bars: 5 mm. S: differences with the SSC group are statistically significant. A: differences with the SSA group are statistically significant. D: differences with the DS group are statistically significant. C: differences with the CC group are statistically significant. \*: differences are statistically significant for all pairwise comparisons between two specific groups of samples. \*\*: differences are statistically significant for all pairwise comparisons between two specific groups of the references to colour in this figure legend, the reader is referred to the web version of this article.)

high diffuse transmittance, with low levels of other parameters such as the diffuse reflectance, absorption and scattering in all sample types. When diffuse transmittance was analyzed, we found very high average levels (above 67 % in all cases), although significant differences were found among the different study groups (Table 1). These results coincide with those of the RMSE analysis showing values above 0.02 for most comparisons (Table 2). However, we found that the morphologies of the spectral distribution curves were very similar for all comparison groups (GFC  $\geq$  0.9992, suggesting very good or excellent spectral matches). In general, the diffuse transmittance exhibited a relatively stable spectral behavior with increasing values at shorter wavelengths, peaking around 555 nm, followed by a slight decrease at longer wavelengths. For the diffuse reflectance, differences were statistically significant for most comparisons when Kruskal-Wallis and Mann-Whitney tests were used (Table 1), although the analysis of the curves using RMSE and GFC suggests an excellent overall coincidence of the curves (RMSE < 2 % for most samples different to P-CC, and GFC values between 0.9940 and 1.0000) (Table 2). As shown in Fig. 2, the spectral behavior was very low and remained stable over the 400-800 nm wavelength range. On the other hand, the comparisons made for the scattering and absorption coefficients found significant differences among groups for both the comparison of average values (Table 1) and spectral distribution curves (RMSE > 2 % and GFC > 0.9006 (Table 2). In general, values were very low for both the scattering and absorption, although a decreasing trend was found for the scattering values as the wavelength increased.

#### 3.3. Analysis of in vivo biocompatibility of FSB

When samples were subcutaneously grafted in laboratory animals, we found that the implant was well tolerated in all study groups. As

shown in Fig. 3, macroscopic assessment of the implant area revealed an apparent good integration of the material at the recipient site, with no gross signs of necrosis, infection, hemorrhage or rejection, comparable to mock animals in which the biomaterial was not implanted. Histologically, we found a local inflammatory reaction with abundant mononuclear cells in all groups, although this reaction was more intense and evident in the SSC and SSA groups and very slight in the CC and mock groups of animals. After the follow-up time, the implanted material was encapsulated by a thin pseudocapsule in all groups. Furthermore, an analysis of the main parameters analyzed in blood of animals grafted with the different materials showed no significant alterations of these parameters. In fact, the levels of each hematological and biochemical marker were similar among groups, with non-significant differences with the mock group (Fig. 3). Finally, the analysis of the inner organs of these animals revealed no alterations in any of these organs, suggesting that the graft was not associated to any detectable systemic alterations (data not shown).

#### 3.4. Histological and optical analysis of cellularized FSB (C-FSB)

When corneal epithelial cells were cultured on the surface of P-FSB, we found that all biomaterials supported cell adhesion and cell differentiation. When C-FSB were histologically analyzed using hematoxylin and eosin and DAPI staining, we found that cells attached to all types of biomaterials, although the level of differentiation and stratification differed among the different C-FSB. As shown in Fig. 4, C-SSA and C-CC achieved the highest levels of epithelial cell stratification and differentiation, as compared to native human corneas used as controls (CTR), whereas the epithelial layer formed on C-SSC and C-DS was formed by a single cell layer. When C-FSB were analyzed using SEM, we found that

Table 1

Analysis of the optical and biomechanical parameters of the native fish scale biomaterials (N-FSB) and preconditioned fish scale biomaterials (P-FSB) analyzed in the present work. SSC: Scorpaena scrofa (red scorpionfish); SSA: Salmo salar (salmon); DS: Diplodus sargus (white sea bream); CC: Cyprinus carpio (European carp). For each species, N- refers to the native biomaterial, whereas P- refers to the preconditioned biomaterial. Values obtained for the optical parameters (diffuse transmittance, reflectance, absorption and scattering) and the biomechanical parameters (Young's modulus, strain at fracture and traction deformation) are shown as averages and standard deviations. P values for the statistical comparison of several groups using the test of Kruskal-Wallis (KW) and the pairwise comparison of two specific groups using the test of Mann-Whitney are shown in the lower rows. Statistically significant p values are highlighted with asterisks (\*).

	Diffuse Transmitance (%)	Diffuse Reflectance (%)	Scattering Coefficient (mm <sup>-1</sup> )	Absorption Coefficient (mm <sup>-1</sup> )	Young's modulus (MPa)	Strain at fracture (N)	Traction deformation (%)
N-SSC	80.86 ± 1.81	$8.42 \pm 0.41$	$1.50\pm0.14$	$0.25\pm0.08$	871.01 ± 311.43	$28.20 \pm 13.42$	$29.09 \pm 9.07$
N-SSA	$80.52 \pm 2.44$	$7.57\pm0.70$	$1.12\pm0.62$	$0.38 \pm 0.15$	304.44 ± 119.51	$48.24 \pm 23.82$	$27.98 \pm 4.12$
N-DS	83.88 ± 1.75	$7.41 \pm 0.52$	$1.63 \pm 0.30$	$0.27 \pm 0.16$	895.08 ± 396.16	61.99 ± 34.29	$24.96 \pm 8.85$
N-CC	67.69 ± 5.36	6.97 ± 1.95	$0.59 \pm 0.10$	$0.35 \pm 0.16$	1481.81 ± 407.04	55.19 ± 17.50	29.27 ± 18.36
P-SSC	$79.81 \pm 2.55$	$5.91 \pm 0.97$	$1.17 \pm 0.18$	$0.53 \pm 0.21$	$67.77 \pm 27.94$	$20.66 \pm 8.30$	$47.86 \pm 15.25$
P-SSA	$81.20 \pm 2.89$	$7.62 \pm 0.85$	$2.03 \pm 0.52$	$0.43 \pm 0.16$	108.23 ± 39.23	14.32 ± 5.95	$21.31 \pm 7.82$
P-DS	77.43 ± 4.96	$6.35 \pm 1.26$	$0.70 \pm 0.23$	$0.32 \pm 0.13$	444.68 ± 133.05	40.67 ± 9.84	$48.00 \pm 21.50$
P-CC	74.62 ± 3.92	$11.46 \pm 1.73$	$0.68\pm0.12$	$0.10 \pm 0.06$	427.02 ± 60.19	99.41 ± 20.43	37.48 ± 11.44
N-FSB KW	<0.0001*	<0.0001*	<0.0001*	<0.0001*	0.0001*	0.0274	0.4415
N-SSC vs. N-SSA	<0.0001*	<0.0001*	<0.0001*	<0.0001*	0.0011	0.1049	0.3823
N-SSC vs. N-DS	<0.0001*	<0.0001*	<0.0001*	0.0047	0.9591	0.0281	0.3282
N-SSC vs. N-CC	<0.0001*	<0.0001*	<0.0001*	<0.0001*	0.0104	0.0030	0.3282
N-SSA vs. N-DS	<0.0001*	<0.0001*	<0.0001*	<0.0001*	0.0019	0.3823	0.3823
N-SSA vs. N-CC	<0.0001*	<0.0001*	<0.0001*	0.0001*	0.0002*	0.2786	0.1949
N-DS vs. N- CC	<0.0001*	<0.0001*	<0.0001*	<0.0001*	0.0047	0.8785	0.9591
P-FSB KW	<0.0001*	<0.0001*	<0.0001*	<0.0001*	<0.0001*	<0.0001*	0.0038
P-SSC vs. P- SSA	<0.0001*	<0.0001*	<0.0001*	<0.0001*	0.0650	0.1304	0.0070
P-SSC vs. P- DS	<0.0001*	<0.0001*	<0.0001*	<0.0001*	0.0002*	0.0011	0.7209
P-SSC vs. P- CC	<0.0001*	<0.0001*	<0.0001*	<0.0001*	0.0002*	0.0002*	0.0830
P-SSA vs. P- DS	<0.0001*	<0.0001*	<0.0001*	<0.0001*	0.0002*	0.0002*	0.0070
P-SSA vs. P- CC	<0.0001*	<0.0001*	<0.0001*	<0.0001*	0.0002*	0.0002*	0.0019
P-DS vs. P- CC	<0.0001*	<0.0001*	<0.0001*	<0.0001*	0.7984	0.0002*	0.1605
N-SSC vs. P-SSC	<0.0001*	<0.0001*	<0.0001*	<0.0001*	0.0002*	0.2786	0.0070
N-SSA vs. P-SSA	<0.0001*	<0.0001*	<0.0001*	<0.0001*	0.0003*	0.0003*	0.0650
N-DS vs. P- DS	<0.0001*	<0.0001*	<0.0001*	<0.0001*	0.0281	0.1949	0.0148
N-CC vs. P- CC	<0.0001*	<0.0001*	<0.0001*	<0.0001*	0.0002*	0.0006*	0.1049

cells formed a tight layer of cells only in C-DS and C-CC, whereas some areas devoid of cells were detected in C-SSC and C-SSA.

Analysis of the gross transparency of C-FSB revealed that all biomaterials were apparently translucent and similar to the control native corneas (CTR). This was confirmed by the analysis of the optical properties of each material (Fig. 4 and Tables 3 and 4), showing high diffuse transmittance and low diffuse reflectance, scattering and absorption in all samples. When the diffuse transmittance of C-FSB was analyzed, we found that this parameter was significantly higher in all C-FSB as compared to CTR across the entire spectral range (400–800 nm) (Table 3). Among the C-FSB samples, C-CC and C-SSA displayed the highest diffuse transmittance values, reaching maximum values of 0.82 and 0.83, respectively, within the intermediate wavelength range. In all cases (CTR and C-FSB), the diffuse transmittance curve was lower for the

lowest wavelengths, and tended to increase at higher wavelengths, with a slight decrease for the highest values of this parameter. To determine the similarity of the different spectral distributions, we used spectral quality metrics (Table 4). In this regard, we found that the diffuse transmittance spectral distribution curves were very similar for all types of C-FSB (C-SSC, C-SSA, C-DS and C-CC), with GFC values above 0.9998 for all comparisons, and RMSE was below 2 % for some specific comparisons. However, the morphology of the spectral distribution curves of C-FSB samples differed to that of CTR as determined by the GFC and RMSE, except for C-CC (GFC =0.9991). For the diffuse reflectance, values were low for all C-FSB samples (<9.5 %), and the spectral distributions were very similar for the four types of C-FSB (RMSE <0.02 and GFC  $\geq0.9922$  for all comparisons), although significant differences were found for the average values, except for the comparison of C-SSA

Table 2
Statistical comparison of the RMSE and GFC results obtained for the native fish scale biomaterials (N-FSB) and preconditioned fish scale biomaterials (P-FSB) analyzed in the present work. SSC: Scorpaena scrofa (red scorpionfish); SSA: Salmo salar (salmon); DS: Diplodus sargus (white sea bream); CC: Cyprinus carpio (European carp). For each species, N- refers to the native biomaterial, whereas P- refers to the preconditioned biomaterial. Values correspond to statistical p values for each comparison between two specific groups of samples. For the RMSE results, values below 0.02 are labeled with an asterisk (\*). For the GFC results, values between 0.9990 and 0.9999 are highlighted with an asterisk (\*), whereas values equal or higher than 0.9999 are labeled with two asterisks (\*\*).

	GFC	N-SSC	N-SSA	N-DS	N-CC	P-SSC	P-SSA	P-DS	P-CC
	RMSE								
	N-SSC	4 0000**	0.0071*	0.0309	0.1332	0.0109*	0.0179*	0.0346	0.0670
	N-SSA	1.0000**	4 0000**	0.0337	0.1309	0.0111*	0.0244	0.0325	0.0663
Diffuse	N-DS	1.0000**	1.0000**	0.0000*	0.1640	0.0416	0.0357	0.0654	0.0974
transmittance	N-CC	0.9995*	0.9993*	0.9993*	0.0000*	0.1226	0.1352	0.0987	0.0699
	P-SSC	1.0000**	0.9999**	0.9999**	0.9996*	0.0000*	0.0206	0.0240	0.0563
	P-SSA	0.9998*	0.9996*	0.9996*	0.9999**	0.9998*	0.0000**	0.0401	0.0661
	P-DS	1.0000**	0.9999**	0.9999**	0.9997*	1.0000**	0.9999**	0.0000*	0.0346
	P-CC	0.9995*	0.9992*	0.9992*	0.9999**	0.9995*	0.9999**	0.9996*	
	GFC RMSE	N-SSC	N-SSA	N-DS	N-CC	P-SSC	P-SSA	P-DS	P-CC
	N-SSC		_ 0.0091*	0.0103*	0.0147*	0.0254	0.0094*	0.0209	0.0306
	N-SSA	0.9993*		0.0028*	0.0068*	0.0177*	0.0070*	0.0129*	0.0390
Diffuse	N-DS	0.9997*	0.9995*		0.0049*	0.0157*	0.0061*	0.0109*	0.0406
reflectance	N-CC	0.9994*	0.9989	0.9995*		_ 0.0116*	0.0086*	0.0068*	0.0451
	P-SSC	0.9973	0.9946	0.9965	0.9967		0.0172*	0.0052*	0.0559
	P-SSA	0.9978	0.9958	0.9972	0.9973	0.9996*		0.0133*	0.0392
	P-DS	0.9992*	0.9979	0.9992*	0.9991*	0.9987	0.9990*		0.0514
	P-CC	0.9992*	0.9998*	0.9994*	0.9988	0.9940	0.9951	0.9975	
	GFC RMSE	N-SSC	N-SSA	N-DS	N-CC	P-SSC	P-SSA	P-DS	P-CC
	N-SSC		0.3865	0.1421	0.9132	0.3452	0.6007	0.7985	0.8228
	N-SSA	0.9982		0.5100	0.5452	0.1665	0.9739	0.4285	0.4515
Scattering	N-DS	0.9993*	0.9994*		1.0458	0.4815	0.5117	0.9301	0.9543
coefficient	N-CC	0.9948	0.9877	0.9913		0.5861	1.4695	0.1194	0.0978
	P-SSC	0.9963	0.9906	0.9937	0.9968		0.8876	0.4735	0.4981
	P-SSA	0.9920	0.9845	0.9884	0.9958	0.9986		1.3588	1.3832
	P-DS	0.9988	0.9947	0.9971	0.9978	0.9986	0.9963		0.0286
	P-CC	0.9990	0.9951	0.9973	0.9975	0.9985	0.9963	0.9998*	
	GFC RMSE	N-SSC	N-SSA	N-DS	N-CC	P-SSC	P-SSA	P-DS	P-CC
	N-SSC		0.1257	0.0533	0.0995	0.2844	0.1935	0.0656	0.1602
Absorption coefficient	N-SSA	0.9974		0.1152	0.0624	0.1612	0.1052	0.0729	0.2836
	N-DS	0.9861	0.9827		0.1153	0.2694	0.1911	0.0806	0.1945
	N-CC	0.9868	0.9907	0.9521		0.2014	0.1257	0.0395	0.2443
	P-SSC	0.9927	0.9969	0.9746	0.9926		0.1567	0.2258	0.4414
	P-SSA	0.9853	0.9788	0.9552	0.9802	0.9687		0.1499	0.3366
	P-DS	0.9934	0.9967	0.9698	0.9970	0.9979	0.9786		0.2164
	P-CC	0.9481	0.9372	0.9006	0.9539	0.9257	0.9867	0.9438	

vs. C-CC. The average values of diffuse reflectance were significantly lower in C-FSB than in native controls, which showed average values < 12 % (Table 3). Comparison of the curve morphology reveals that C-SSC and C-SSA were very similar to CTR, as determined by the GFC parameter (0.9990 vs. C-SSC and 0.9999 vs. C-SSA), although the RMSE was above 0.02 for all C-FSB compared with CTR. Furthermore, our results showed low average values for the scattering and, especially, for the absorption coefficients in C-FSB and CTR samples. For both parameters, a decreasing spectral trend was found as the wavelength increased (Fig. 4). For the scattering coefficient, all C-FSB samples were significantly higher than CTR, and the highest scattering levels corresponded to C-SSC and C-SSA, especially at the shorter wavelengths. The same trend was found for the absorption coefficient, although less differences among samples were detected in this case. For both the absorption and scattering coefficients, the quality metrics indicated similar spectral behaviors (GFC > 0.9903 for scattering and GFC > 0.9911 for absorption), but significant scale differences (RMSE > 2 %).

In order to determine the differentiation level of the epithelial layer, we analyzed the expression of relevant differentiation markers in these cells. Results of these analyses (Fig. 5 and Table 5) showed partial similitudes between CTR corneas and C-FSB, although none of the C-FSB expressed the same levels of these markers as CTR. Specifically, we first

found that the expression of cytokeratins AE1/AE3 was strongly positive in CTR and in C-SSC, whereas C-SSA, C-DS and C-CC had a positive signal for this marker. For CRY- $\alpha A$ , our results showed a strongly positive signal in CTR and C-DS and a very positive signal in C-SSC, C-SSA and C-CC. For the limbal stem cell marker  $\Delta Np63$ , our results showed a very positive signal in CTR, C-SSC and C-CC, whilst C-SSA and C-DS were positive. Then, analysis of the intercellular junction protein TJP1 revealed a strong positive signal in CTR and C-SSA, a very positive signal in C-DS and a positive immunostaining signal for C-SSC and C-CC. Finally, the analysis of protein expression of the cell proliferation marker KI67 showed a slightly positive signal in CTR samples, but it was strongly positive in C-DS and C-CC and very positive in C-SSC and C-SSA (Fig. 5 and Table 5).

These expression patterns correlated with some of the physical parameters analyzed in this study. Specifically, we found that the highest expression of the cell differentiation marker  $\Delta Np63$  corresponded to FSB samples showing the highest values of reflectance. In addition, cell proliferation assessed by KI67 immunohistochemistry, was higher in samples with the highest Young's modulus and strain at fracture, but lower in samples with the lowest scattering and absorption values.

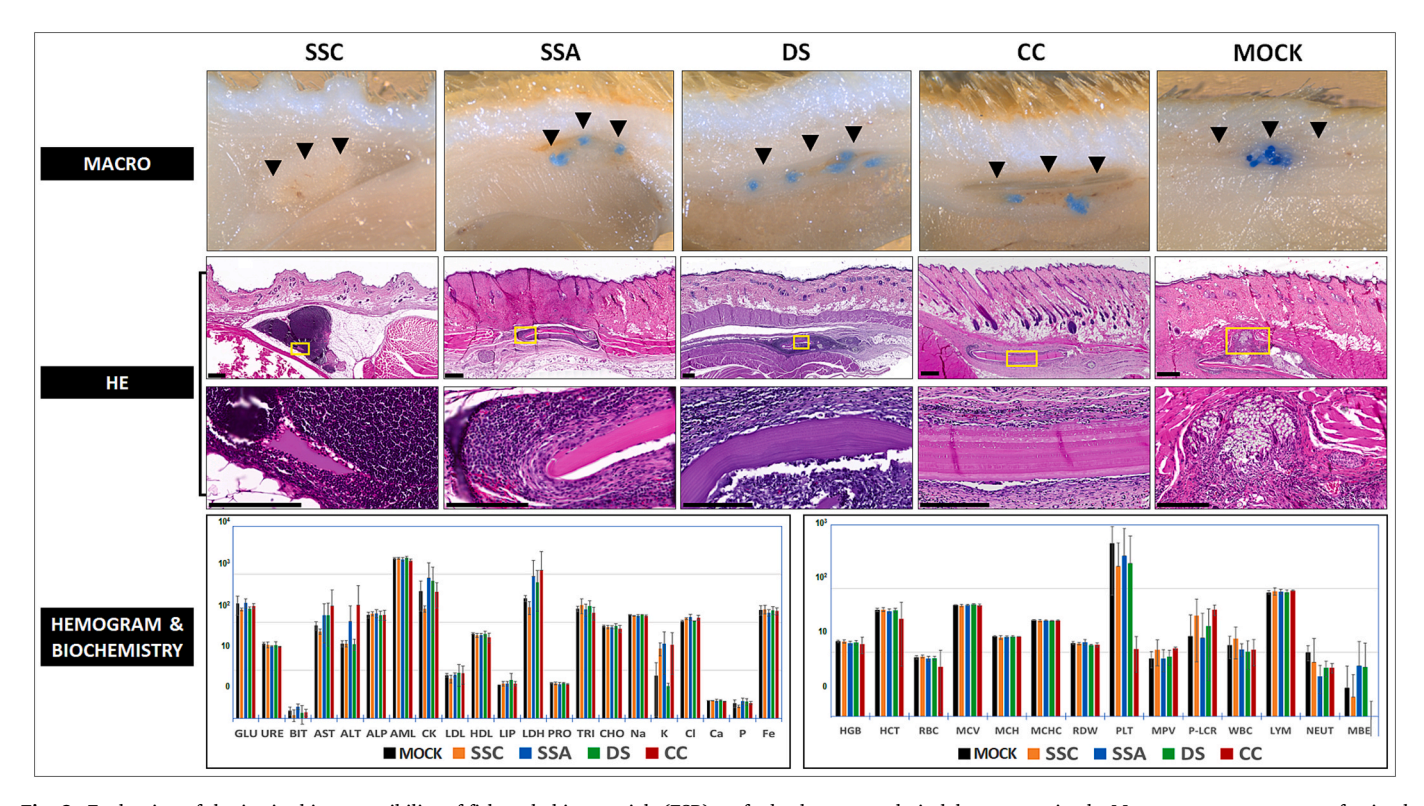


Fig. 3. Evaluation of the *in vivo* biocompatibility of fish scale biomaterials (FSB) grafted subcutaneously in laboratory animals. Macro: gross appearance of animal tissues in which the FSB were implanted. Black arrowheads highlight the grafting area, with suture material seen in some cases in blue. HE: histological analysis of the grafting area using hematoxylin and eosin staining at two different magnifications. Bottom images correspond to a magnification of the areas shown with yellow squares in the top images, with the scale bars corresponding to 500 μm in the top images and 200 μm in the high-magnification images. SSC: *Scorpaena scrofa* (red scorpionfish); SSA: *Salmo salar* (salmon); DS: *Diplodus sargus* (white sea bream); CC: *Cyprinus carpio* (European carp); Mock: control animals in which a FSB was not grafted. Hemogram and serum biochemistry: results of the quantitative analysis of major parameters evaluated in blood of the animals grafted with FSB. Histograms correspond to average and standard deviation values. GLU: glucose (mg/dL), URE: urea (mg/dL), BIT: total bilirubin (μmol/L), AST: aspartate transaminase (U/L), ALT: alanine transaminase (U/L), ALP: alkaline phosphatase (U/L), AML: anylase (U/L), CK: creatine kinase (U/L), LDL: low-density lipoprotein (mg/dL), HDL: high-density lipoprotein (mg/dL), LIP: lipase (U/L), LDH: lactate dehydrogenase (U/L), PRO: total proteins (g/dL), TRI: triglycerides (mg/dL), CHO: cholesterol (mg/dL), Na: sodium (mmol/L), K: potassium (mmol/L), Cl: chlorine (mmol/L), Ca: calcium (mmol/L), P: phosphorous (mmol/L), Fe: iron (μg/dL), HGB: hemoglobin (g/dL), NGCH: mean corpuscular hemoglobin (pg), MCHC: mean red blood cells (10<sup>6</sup>/μL<sup>-1</sup>), MCV: mean red lood cells (10<sup>6</sup>/μL<sup>-1</sup>), MCV: mean red lood cells (10<sup>8</sup>/μL<sup>-1</sup>), LYM: percentage of lymphocytes (%), NEUT: percentage of neutrophils (%), MBE: percentage of monocytes–basophils–eosinophils (%). Differences with control animals (mock) are not statistically significant (p > 0.05). (For interpretation of the referenc

#### 3.5. In vivo evaluation of FSB grafted in the cornea of laboratory animals

When CC biomaterials were implanted intrastromally in the cornea of laboratory rabbits, we found that these FSB became integrated in the host cornea, and we found no signs of neovascularization, infection, rejection, or other complications, comparable to native corneas devoid of the implant (Fig. 6). At the macroscopic level, we found that the graft stayed at the grafting site of the host cornea after 1 and 3 months of follow-up. At the moment of the euthanasia, after 3 months of the implant, the host cornea was devoid of any detectable side effects, and its gross appearance was similar to the native cornea, with the exception of the implant, that could be detected within the cornea stroma using the slit lamp. These findings were in agreement with the OCT results showing a normal structure of the host cornea, with a dense biomaterial integrated within the stroma. No blood vessels, inflammation or other possible complications were detected in any of the animals.

To confirm these results, we carried out histological, histochemical and immunohistochemical studies of the corneas grafted with the CC FSB and native corneas used as controls. Results are shown in Fig. 7 and Table 6 and demonstrate that the biomaterial remained within the corneal stroma, and no inflammation or other complications were detected. The absence of neovascularization in the host cornea was confirmed by immunohistochemistry for the endothelial cell marker

CD34, which was negative in both the native cornea and the cornea grafted with the CC biomaterial. In addition, the analysis of expression of cytokeratin CK3, CRY- $\alpha$ A and  $\Delta$ Np63 confirmed that the implant of this FSB was not associated with an alteration of the normal physiology of the corneal epithelial cells, as expression of these three markers was similar in native corneas and in corneas grafted with CC (strongly positive for CK3 and CRY- $\alpha$ A, and very positive for  $\Delta$ Np63). Finally, the analysis of three relevant components of the corneal stroma ECM (collagen fibers, proteoglycans and lumican) revealed that the presence of the biomaterial was associated with a slight increment in the signal intensity of collagen and lumican, although not for proteoglycans, which were to native corneas (Fig. 7 and Table 6).

#### 4. Discussion

Development of novel biomaterials with potential usefulness in biomedicine is one of the main objectives of current tissue engineering [16,17,35]. In the present work, we generated and characterized several types of FSB obtained from four fish species that had not been reported to the date. The fact that these four species have important commercial value as common fish found in most local markets worldwide ensures easy access to the sources of raw material for the generation of these novel products. Interestingly, our initial analysis of native materials

I. Garzón et al. Materials & Design 258 (2025) 114703

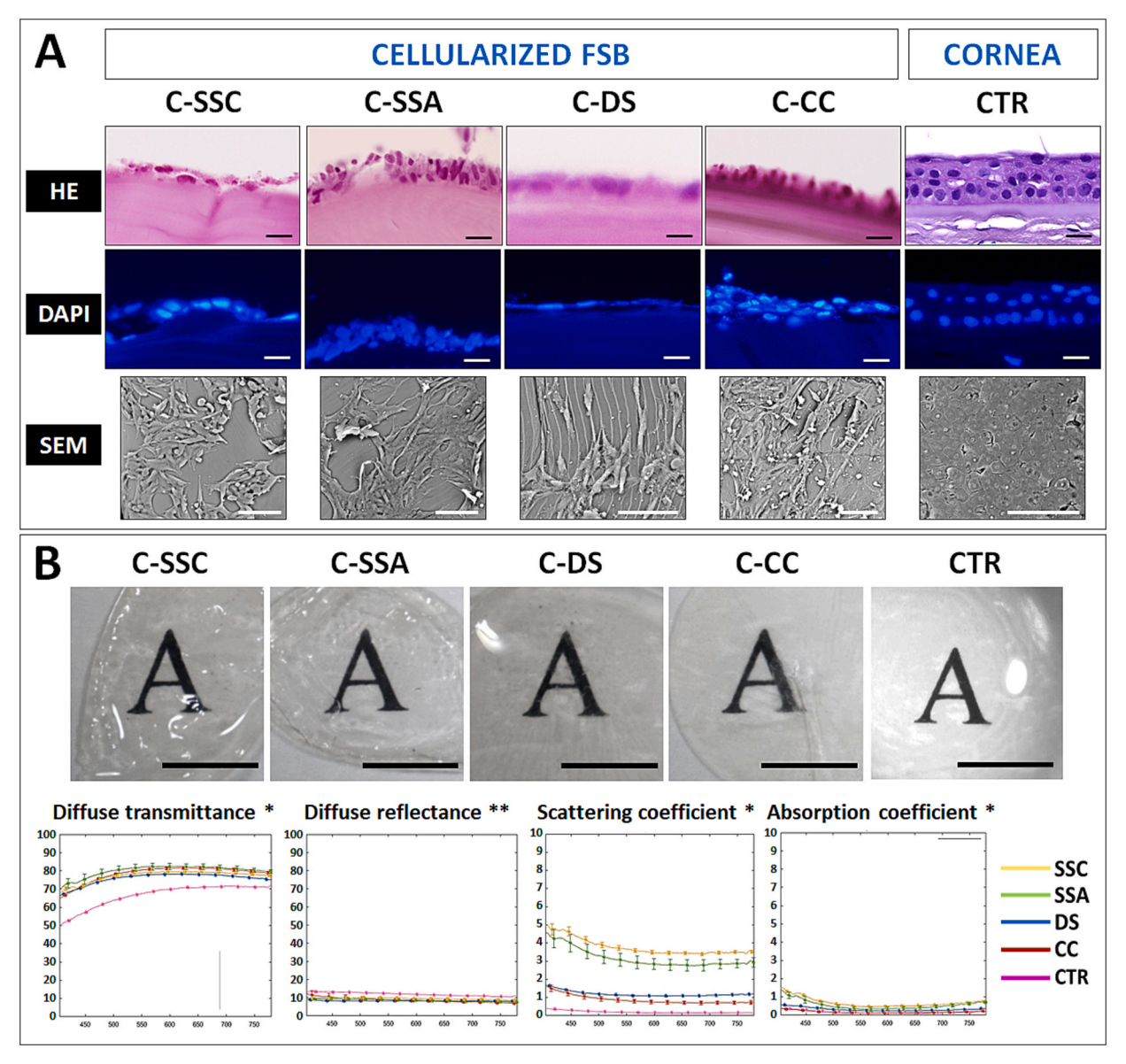


Fig. 4. Characterization of cellularized fish scale biomaterials (C-FSB) and control native corneas (CTR). A: histological analysis using hematoxylin and eosin staining (HE), DAPI staining (DAPI) and scanning electron microscopy (SEM). B: analysis of optical properties as determined by the gross translucency of each sample on a black printed letter (top panels) and by analyzing the diffuse transmittance, diffuse reflectance, scattering and absorption coefficient (lower panels). SSC: Scorpaena scrofa (red scorpionfish); SSA: Salmo salar (salmon); DS: Diplodus sargus (white sea bream); CC: Cyprinus carpio (European carp). Scale bars: 20 µm in panel A and 5 mm in panel B. \*: differences are statistically significant for all pairwise comparisons between two specific groups of samples. \*\*: differences are statistically significant for all pairwise comparisons between two specific groups of samples, except for C-SSA vs. C-CC. (For interpretation of the references to colour in this figure legend, the reader is referred to the web version of this article.)

revealed important differences among species. Specifically, we found that N-SSA was very thick, as compared to the rest of N-FSB, whereas N-DS was very thin. In addition, N-CC contained a high amount of fish cells, whereas cells in N-SSA and N-DS were very scarce, and N-CC showed a more heterogeneous multi-laminar structure as compared to the rest of the scales. Despite most previous studies were carried out using the same source of fish scales [36–38], these morphological and structural differences which reinforce the need to develop this type of comparative studies among fish species to find the most appropriate product for future clinical use.

In the first place, fish scales obtained from the different species of fish were subjected to preconditioning in order to optimize their biological properties and minimize potential side effects derived from the presence of fish cells and calcium deposits using acid incubation protocols, as previously reported [38]. The use of these protocols resulted in a very

effective decellularization and decalcification, with no rests of cells or calcium deposits found in any of the P-FSB, without altering the structure of the biomaterial or its collagen composition revealed by PSR histochemical staining. Although specific immunohistochemical analyses should be carried out to identify specific types of collagen before and after preconditioning, PSR analysis suggest that collagen was not significantly altered by preconditioning. Albeit PSR is not highly specific, this method has been shown to reliable identify most collagen types across virtually all animal species, without the interspecific variability inherent to immunohistochemistry [39]. However, preconditioning was associated with a significant modification of the biomechanical properties of FSB, with a reduction in the Young's modulus in P-SSC, P-SSA and P-CC and an increase in the strain at fracture in P-CC. This modification is probably associated with the loss of the mineralized layer that was originally associated to the N-FSB, as it

Table 3

Analysis of the optical parameters of control native corneas (CTR) and cellularized fish scale biomaterials (C-FSB) analyzed in the present work. SSC: Scorpaena scrofa (red scorpionfish); SSA: Salmo salar (salmon); DS: Diplodus sargus (white sea bream); CC: Cyprinus carpio (European carp). Values obtained for the diffuse transmittance, diffuse reflectance, scattering and absorption coefficients are shown as averages and standard deviations. P values for the statistical comparison all C-FSB groups using the test of Kruskal-Wallis (KW) and the pairwise comparison of two specific groups using the test of Mann-Whitney are shown in the lower rows. Statistically significant p values are highlighted with asterisks (\*).

with aster	11010 ( ).			
	Diffuse Transmitance (%)	Diffuse Reflectance (%)	Scattering Coefficient (mm <sup>-1</sup> )	Absorption Coefficient (mm <sup>-1</sup> )
	· ·		· · ·	, ,
CTR	66.6 ± 6.06	$11.94 \pm 0.91$	$0.94 \pm 0.22$	$0.2 \pm 0.06$
C-SSC	$77.25 \pm 3.3$	$9.49 \pm 0.51$	$3.77 \pm 0.53$	$0.69 \pm 0.26$
C-SSA	$80.07 \pm 3.04$	$8.6 \pm 0.63$	$3.16 \pm 0.51$	$0.56 \pm 0.24$
C-DS	$75.81 \pm 3.01$	$8.29 \pm 0.26$	$1.19 \pm 0.17$	$0.32 \pm 0.09$
C-CC	$78.4 \pm 4.24$	$8.77 \pm 1.52$	$0.88 \pm 0.26$	$0.17 \pm 0.07$
C-FSB	<0.0001*	<0.0001*	<0.0001*	<0.0001*
KW				
CTR	<0.0001*	<0.0001*	<0.0001*	<0.0001*
vs.				
C-				
SSC				
CTR	<0.0001*	<0.0001*	<0.0001*	<0.0001*
vs.				
C-				
SSA				
CTR	<0.0001*	<0.0001*	<0.0001*	<0.0001*
vs.				
C-				
DS				
CTR	<0.0001*	<0.0001*	<0.0001*	<0.0001*
vs.				
C-				
CC				
C-SSC	<0.0001*	<0.0001*	<0.0001*	<0.0001*
vs.				
C-				
SSA				
C-SSC	<0.0001*	<0.0001*	<0.0001*	<0.0001*
vs.				
C-				
DS				
C-SSC	<0.0001*	<0.0001*	<0.0001*	<0.0001*
vs.				
C-				
CC				
C-SSA	<0.0001*	<0.0001*	<0.0001*	<0.0001*
vs.				
C-				
DS				
C-SSA	<0.0001*	0.3057	<0.0001*	<0.0001*
vs.				
C-				
CC				
C-DS	<0.0001*	<0.0001*	<0.0001*	<0.0001*
vs.				
C-				
CC				

is well known that mineralized material typically shows high stiffness and low elasticity as compared to soft tissues [40]. Although there are no consensus values, previous studies demonstrated that the human native cornea biomechanical properties may range between 0.8–2.2 MPa [41] and approximately 100 MPa [29] for the Young's modulus, and approximately 5 N for the strain at fracture [29]. In our study, preconditioning was able to reduce the high values Young's modulus found in native materials, with the added advantage of increasing the elasticity of the material as determined by the strain at fracture, in the case of P-CC. As a viscoelastic tissue, elasticity of the human cornea is one of the most crucial biomechanical parameters of this organ [41], and biomaterials intended for use in corneal repair should also be viscoelastic.

However, the results found in the present study showed high variability as determined by a high standard deviation. Although variability is a common characteristic of biological tissues analyzed biomechanically [42], our results should be taken with caution, and future studies should be carried out using a larger sample size.

Regarding transparency, we found that all FSB evaluated in the present work were very translucid, especially after the mineralized structures were removed by preconditioning, and cellularized biomaterials kept these gross transparency levels. In addition, our analysis of the optical behavior confirmed the excellent levels of transparency displayed by FSB. In general, FSB showed high transmittance of light, with low levels of reflectance, scattering and absorption, suggesting that these novel materials may fulfill the optical requirements for use in corneal repair and engineering, as optical performance is pivotal for application of novel biomaterials in corneal tissue engineering [43]. An interesting finding of our work was an increase diffuse reflectance in CC biomaterials subjected to preconditioning. Although differences were not statistically significant, this increase could be a consequence of the trend of P-CC to reduce surface roughness, likely due to the loss of mineralized particles at the material surface, as it is well known that rough surfaces typically show reduced reflectance levels [44].

One factor that may influence the optical properties of FSB is the Ca/P ratio, which has been directly associated with the optical properties of biological materials [45]. It has been previously demonstrated that the Ca/P ratio for scales derived from SSA, DS and a species related to CC are 1.94 [46], 1.80 [47] and 2.01 [48], respectively, while SSC scales are estimated to have a ratio close to 1.90 [49]. Interestingly, these Ca/P ratios showed an inverse relationship with the light transmittance and scattering results obtained in N-FBS, with the highest optical transparency values observed in scales exhibiting the lowest Ca/P ratios. It is known that stoichiometric hydroxyapatite has a Ca/P ratio of 1.67 and tends to be a highly crystalline and highly transparent [50]. Accordingly, it was not unexpected that an increase in Ca/P ratio was associated with a reduction in light transmittance and an impairment in the optical properties of FBS biomaterials.

Not only the N-FSB and P-FSB, but also the biomaterials subjected to cellularization (C-FSB) displayed adequate optical properties for use in tissue engineering. In fact, our quantitative analyses demonstrated that C-FSB samples possessed significantly higher transmittance than CTR across the visible spectrum (400-800 nm), especially, at the lowest wavelengths. This excellent transmittance may be explained by the low levels of reflectance, scattering and absorption shown by all samples, suggesting that most of the incoming light is transmitted throughout the biomaterial with minimal loss of light, as is the case of CTR tissues. For C-FSB, we found that the lowest scattering and absorption levels, which account for most of the loss of transparency in biological tissues [51], corresponded to CC biomaterials (N-CC, P-CC and C-CC), suggesting that these scales could have the highest intrinsic potential for use in cornea tissue engineering. In addition, FSB biomaterials displayed a wavelength-dependent transmittance profile that might allow for further customization in clinical settings. Collectively, the optical properties displayed by the FSB analyzed in the present work, including enhanced transmittance, low reflectance, controlled scattering, and minimal absorption, support the potential of these biomaterials to mimic the optical properties of the human cornea, as previously reported for biomaterials used in cornea tissue engineering [2].

A very important requirement of biomaterials intended for clinical use in advanced therapies is a thorough characterization of the new products, including several quality controls to ensure that these materials are safe once grafted in a human patient [52]. For this reason, we evaluated the novel FSB generated in this work at the *ex vivo* and *in vivo* levels to determine their clinical potential as advanced therapies medicinal products in cornea repair. Results demonstrated that these novel biomaterials support epithelial cell growth and development, and two of the materials (C-SSA and C-CC) achieved in the generation of a stratified epithelium, similar to the native cornea, thus confirming the *ex vivo* 

#### Table 4

Statistical comparison of the RMSE and GFC results obtained for the cellularized fish scale biomaterials (C-FSB) analyzed in the present work. SSC: *Scorpaena scrofa* (red scorpionfish); SSA: *Salmo salar* (salmon); DS: *Diplodus sargus* (white sea bream); CC: *Cyprinus carpio* (European carp). For each species, Values correspond to statistical p values for each comparison between two specific groups of samples. For the RMSE results, values below 0.02 are labeled with an asterisk (\*). For the GFC results, values between 0.9990 and 0.9999 are highlighted with an asterisk (\*), whereas values equal or higher than 0.9999 are labeled with two asterisks (\*\*).

	OFF DWGE	0.000	0.004	0.00	0.00	OTD
	GFC RMSE	C-SSC	C-SSA	C-DS	C-CC	CTR
	C-SSC		0.0283	0.0149*	0.0178*	0.1119
Diffuse	C-SSA	1.0000**		0.0426	0.0212	0.1392
transmittance	C-DS	1.0000**	1.0000**		0.0291	0.0986
	C-CC	0.9999**	0.9998*	0.9999**		0.1205
	CTR	0.9984	0.9983	0.9984	0.9991*	
	GFC RMSE	C-SSC	C-SSA	C-DS	C-CC	CTR
	C-SSC		0.0093*	0.0126*	0.0120*	0.0252
Diffuse	C-SSA	0.9995*		0.0061*	0.0074*	0.0336
reflectance	C-DS	0.9991*	0.9981		0.0121*	0.0374
	C-CC	0.9939	0.9968	0.9922		0.032
	CTR	0.9990*	0.9999**	0.9979	0.9976	
	GFC RMSE	C-SSC	C-SSA	C-DS	C-CC	CTR
	C-SSC		0.613	2.5987	2.8978	2.8337
Scattering	C-SSA	0.9992*		2.0033	2.2961	2.2332
coefficient	C-DS	0.9992*	0.9986		0.3257	0.2663
	C-CC	0.9903	0.9947	0.9896		0.0739
	CTR	0.9937	0.9968	0.9918	0.999	
	GFC RMSE	C-SSC	C-SSA	C-DS	C-CC	CTR
	C-SSC		0.1396	0.3976	0.5465	0.5209
Absorption	C-SSA	0.9965		0.2762	0.4181	0.397
coefficient	C-DS	0.9959	0.9875		0.1537	0.126
	C-CC	0.997	0.998	0.9926		0.0464
	CTR	0.9911	0.9785	0.995	0.9823	

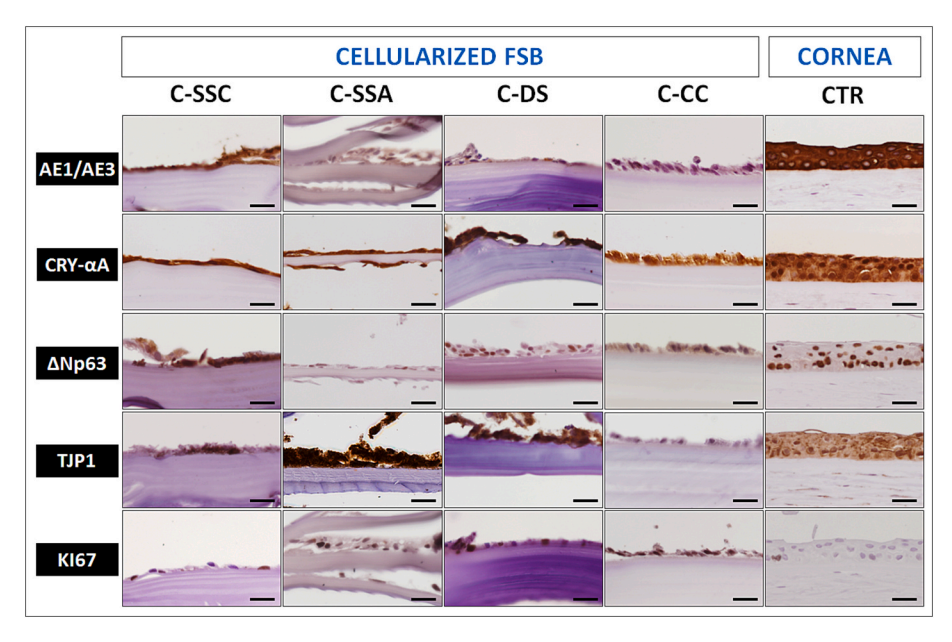


Fig. 5. Immunohistochemical analysis of cellularized fish scale biomaterials (C-FSB) and control native corneas (CTR). Several markers of corneal epithelial differentiation were analyzed, including cytokeratins AE1/AE3, crystallin alpha-A (CRY-αA), the limbal isoform of the protein p63 (ΔNp63), tight-junction protein 1 (TJP1), along with the cell proliferation marker KI67. SSC: *Scorpaena scrofa* (red scorpionfish); SSA: *Salmo salar* (salmon); DS: *Diplodus sargus* (white sea bream); CC: *Cyprinus carpio* (European carp). Scale bars: 50 μm. (For interpretation of the references to colour in this figure legend, the reader is referred to the web version of this article.)

biocompatibility of FSB for use with corneal cells. Importantly, the presence of cells kept the excellent levels of transparency and the optical properties of C-FSB. Although cells cultured with the FSB showed very good biocompatibility, future works should be carried out to determine the effects of these biomaterials on cell cultures, as previously suggested for other types of biomaterials described for use in tissue engineering [53].

When these materials were grafted subcutaneously in laboratory rats, we found no significant alterations in these animals, both in the internal organs and in major blood parameters, confirming that these biomaterials were also biocompatible *in vivo*. Biocompatibility in animals is one of the major requirements of the National Medicines

Agencies for the characterization of novel advanced therapies for future clinical translation [54]. Strikingly, the local reaction of the FSB grafted subcutaneously confirmed that the implant was safe for the animals, and only a localized inflammatory reaction was found locally, that was very mild in the case of the CC. Furthermore, we found that the implant remained stable after 30 days of follow-up, suggesting that *in vivo* biodegradation of these materials is very slow. Given the low regeneration potential of the human cornea [55], temporal stability is one of the requirements of biomaterials grafted in this organ. However, long-term studies should be carried out in the future to determine the fate of FSB grafted subcutaneously in laboratory animals after longer periods of time. In this regard, several reports showed that collagen sponge

#### Table 5

Results of the immunohistochemical analysis of cellularized fish scale biomaterials (C-FSB) and control native corneas (CTR) for cytokeratins AE1/AE3, crystallin alpha-A (CRY- $\alpha$ A), the limbal isoform of the protein p63 ( $\Delta$ Np63), tight-junction protein 1 (TJP1), and the cell proliferation marker KI67. SSC: Scorpaena scrofa (red scorpionfish); SSA: Salmo salar (salmon); DS: Diplodus sargus (white sea bream); CC: Cyprinus carpio (European carp). Results were categorized as negative (-), slightly positive (+/-), positive (+), very positive (++), or strongly positive (+++).

	C-SSC	C-SSA	C-DS	C-CC	CTR
AE1/AE3	+++	+	+	+	+++
CRY-αA	++	++	+++	++	+++
ΔNp63	++	+	+	++	++
TJP1	+	+++	++	+	+++
KI67	++	++	+++	+++	+/-

hydrogels generated from fish skin collagen extraction and jellification tended to become reabsorbed after a few weeks of *in vivo* implantation. similar to collagen hydrogels generated from mammal skin, although most studies were carried out only up to 4 weeks of follow-up [56,57]. One of the few previous works evaluating the long-term stability of fish scales grafted subcutaneously demonstrated that most of the scale remain stable at the grafting site after 11 weeks of the implant [36]. Although these results should be confirmed at longer follow-up times, it is likely that the densely packed, well-organized structure of the fish scale, which significantly differs from the collagen sponges, resulting in a highly stable biomaterial. On the other hand, it has been suggested that decellularized tilapia fish scales might develop an external layer of mineralized material under certain conditions [58]. Although we did not find this phenomenon in FSB grafted in vivo, future works should determine if the FSB may undergo mineralization after several months of in vivo grafting.

When the physiological profile of the cells cultured on C-FSB was

analyzed, we found that FSB biomaterials supported partial differentiation of epithelial cells, with a positive expression of several markers of differentiation found in the normal cornea, such as AE1/AE3, CRY-αA, ΔNp63 and TJP1 [59]. This expression was comparable or even higher than that found in NANOULCOR bioartificial corneas generated with fibrin-agarose and approved for clinical use in Spain [9,31]. However, ex vivo culture of C-FSB was not able to induce terminal differentiation comparable to the native human cornea. This finding is not unexpected, as previous studies demonstrated that the in vivo setting is essential for the artificial tissues to undergo full differentiation in response to the numerous paracrine and endocrine signals and factors that are released by the host tissues [60]. Strikingly, we found that some properties of the FSB biomaterials tended to correlate with cell differentiation and cell proliferation, as previously demonstrated for different types of biomaterials cultured in the presence of cells [61]. Despite these findings should be corroborated by future studies with larger sample size, we found that corneal stem cell differentiation as determined by  $\Delta Np63$ expression tended to correlate with some optical parameters, whereas cell proliferation was associated with the biomechanical results, as previously suggested [62]. An interesting finding was the fact that the highest CRY-αA expression was observed in C-DS. Although the underlying reasons remain unclear, the fact that preconditioned DS scales exhibited the highest Young's modulus after preconditioning suggests that CRY-αA expression could be induced by the biomechanical properties of the biomaterials. In line with this, interesting previous reports demonstrated that corneal strain can significantly influence the expression of relevant corneal proteins, including different types of crystallins [63].

Compared to the native cornea, C-FSB showed a high level of cell proliferation revealed by KI67 expression. As for the cell differentiation markers, it has been previously demonstrated that cells and tissues maintained *ex vivo* tend to show higher cell proliferation levels, and the

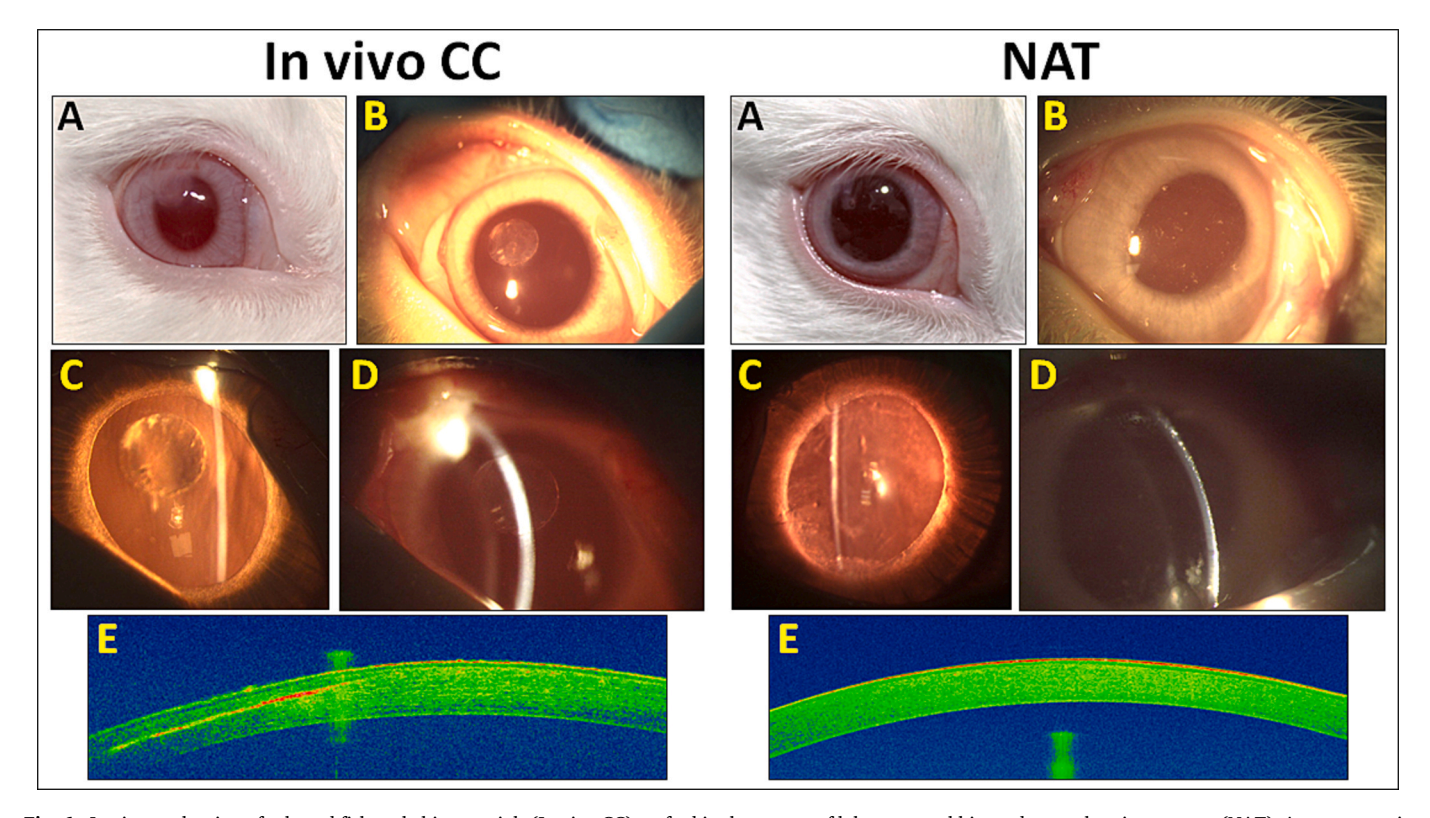


Fig. 6. In vivo evaluation of selected fish scale biomaterials (In vivo CC) grafted in the cornea of laboratory rabbits and control native corneas (NAT). A: macroscopic image of the rabbit cornea 1 month after the implant; B: macroscopic image of the rabbit cornea 3 months after the implant; C and D: slit lamp images of the cornea obtained 3 months after the implant; E: optical coherence tomography (OCT) 3 months after the implant. In vivo CC: animals in which the *Cyprinus carpio* (European carp) FSB were implanted; NAT: native control animals in which no materials were implanted.

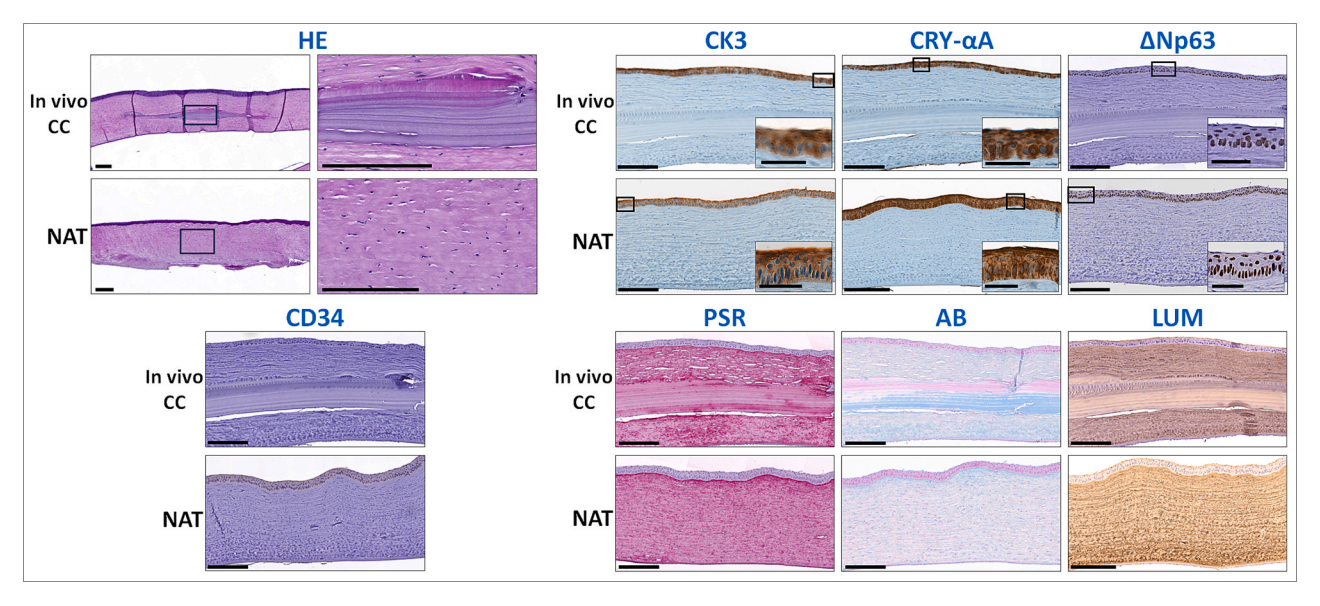


Fig. 7. Histological, histochemical and immunohistochemical analysis of selected fish scale biomaterials (In vivo CC) grafted for 3 months in the cornea of laboratory rabbits and control native corneas in which no materials were implanted (NAT). In both types of corneas, we analyzed the general structure, using hematoxylin and eosin staining (HE) at two magnifications, the presence of neovascular structures by CD34 immunohistochemistry, the epithelial markers cytokeratin 3 (CK3), crystallin alpha-A (CRY-αA), and the limbal isoform of the protein p63 (ΔNp63), and the stromal components collagen (as determined by picrosirius red histochemistry -PSR-), proteoglycans (as determined by alcian blue histochemistry -AB-) and lumican (as determined by immunohistochemistry -LUM-). Scale bars: 200 μm, except for the inserts in CK3, CRY-αA and ΔNp63, corresponding to 50 μm. (For interpretation of the references to colour in this figure legend, the reader is referred to the web version of this article.)

Table 6

Results of the histochemical and immunohistochemical analysis of selected fish scale biomaterials (In vivo CC) grafted for 3 months in the cornea of laboratory rabbits and control native corneas (NAT) for crystallin alpha-A (CRY- $\alpha$ A), the limbal isoform of the protein p63 ( $\Delta$ Np63), cytokeratin 3 (CK3), the vascular endothelial marker CD34, picrosirius red (PSR), alcian blue (AB) and lumican (LUM). Results were categorized as negative (–), slightly positive (+/–), positive (+), very positive (++), or strongly positive (+++).

	In vivo CC	NAT
СКЗ	+++	+++
CRY-αA	+++	+++
ΔNp63	++	++
CD34	_	_
PSR	+++	++
AB	+	+
LUM	+++	++

controlled local release of growth factors can modify cell physiology, differentiation and proliferation [64]. In the specific case of C-CC, we found that cells tended to display high expression of KI67 and lower levels of epithelial differentiation markers such as cytokeratin AE1/AE3 and the intercellular junction protein TJP1. These findings may imply that the CC biomaterial might favor an intermediate cell phenotype rather than a fully-differentiated structure as long as bioengineered tissues are kept *ex vivo*. A similar situation was found in several bioartificial tissues previously generated by tissue engineering, and the partially undifferentiated status of these tissues favored clinical integration in the host tissues when grafted in patients [9,65].

Once we evaluated the four types of FSB generated in this work, we selected the CC biomaterial for intracorneal implant. Although the four FSB showed promising results, selection of CC was based on the results discussed above. On the one hand, our initial characterization of N-CC revealed that the structure of this material might be appropriate for clinical use in cornea repair, and this product naturally associated to a stratified epithelial cell layer developed on top. After preconditioning, P-CC supported cell attachment and growth, with the development of a dense stratified epithelial layer more efficiently than P-SSC, C-SSA and

C-DS. In addition, the P-FSB showing the most appropriate biomechanical results in terms of stiffness and elasticity was P-CC, without altering the excellent levels of transparency and optical properties of these materials. Finally, the in vivo subcutaneous implant in laboratory rats demonstrated that the FSB showing the best biocompatibility was CC, which supports again the use of this biomaterial in cornea repair and engineering. The reasons why CC FSB showed the most adequate results remains elusive. On the one hand, it has been demonstrated that scales of Cyprinid fish are relatively larger than those of the other species analyzed in the present work, and that the specific structure of the scales of each fish species can be used for the taxonomical identification of fish individuals [66]. On the other hand, previous reports found that the microstructure and biochemical composition of fish scales may differ among groups of fish, especially regarding the alignment of the collagen fibrils [67]. Although most cycloid scales, including CC scales, show numerous parallel latices of collagen fibrils axially aligned to the surface of the scale forming a plywood pattern [67], CC scales microstructure is similar to twisted plywood, in which collagen fibrils form lamellae with different orientations that could be responsible for maintaining the integrity and stability of the scale [68]. In addition, ultrastructural analyses using electron microscopy found that CC scales contain an additional array of collagen fibrils, secondary to the main collagen fibers, that has not been identified in other fish species [68].

Intracorneal implant of selected FSB obtained from CC resulted in excellent levels of biocompatibility on the host cornea. Not only the implants were very well tolerated by all animals, without any detectable complications or side effects, but also the biomaterial remained stable in the cornea for at least 3 months without apparently affecting the corneal tissue. Stability and biocompatibility are important requirements of biomaterials for use in corneal repair, and fulfilling these properties is one of the requisites for future clinical translation [69]. Although future studies should evaluate the long-term evolution of FSB grafted in the corneal stroma, it has been reported that the structural stability of fish scales implanted in the rabbit eye could exceed one year [36]. Despite the absence of a control group receiving a gold-standard implant, the compatibility of the FSB was comparable to that of human bioengineered corneas grafted in laboratory rabbits, according to previous

I. Garzón et al. Materials & Design 258 (2025) 114703

reports by our group [54,60], and support the use of the novel FSB products described in the present work.

Furthermore, we demonstrated that the corneal implant was not associated with neovascularization or any structural alteration of the host corneas. In fact, the animal cornea kept normal levels of expression of relevant differentiation markers, including cytokeratins and relevant markers of corneal epithelium differentiation and function such as  $\Delta$ Np63 and CRY- $\alpha$ A [59,70]. However, rabbit corneas grafted with the CC-derived FSB showed a modification of two relevant ECM components -collagen and lumican-, although other components such as proteoglycans were not affected. As one of the major responsible of light transmission, the ECM plays a very important role in the normal physiology of the corneal stroma [71]. Although the consequences of the slight modification of these ECM components remain unknown, it has been demonstrated that corneal surgery is frequently associated with a ECM alteration [72], but it is likely that this alteration could be temporary and self-limited, as we found that the function and transparency of these corneas was not affected by the implant.

Regarding the potential immunogenic effects of FSB grafted *in vivo*, our results showing no excessive inflammation at the implant area are in agreement with previous works reporting the safe use of fish scale-derived biomaterials [36], and the use of collagen sponges fabricated from fish skin demonstrated to be well tolerated by different species of mammals, despite the phylogenetic distance that exists among species [73]. Again, long-term analyses are in need to demonstrate the immunogenic potential of the novel biomaterials described in this work.

To date, very few studies focused on fabricating artificial corneas using blue biomaterials. Along with the scientific and biomedical potential of these materials, the use of the FSB described in this work may have important social and environmental advantages, such as reinforcement of an important economic activity in the European Union and reduction of waste production in fishery and aquaculture, which is still very high [74]. Likewise, the search of methods allowing a more efficient use of fish processing by-products should be a common objective of the fishing and aquaculture industry [75], reducing the ecological impact of these activities while contributing to the development of sustainable medicines [76]. Due to the fact that only three fish species have been previously evaluated as a source of FSB [25], with only one of them being characterized ex vivo and in vivo, the present study provides new evidences on the putative usefulness of these types of biomaterials. As compared to previous studies, the FSB generated in the present work were evaluated at different levels, including biomechanical, optical, histological and functional analyses ex vivo and in vivo, whereas most previous studies were partial and lack some of these analyses, especially regarding a complete optical characterization [25].

As a primary source of material, fish scales are highly available at large scale, as byproducts of the fishing and fish farming factory. Production of fish for human consumption has been efficiently scaled, and large amounts of fish can now be produced in specific fish farms worldwide [77]. Scalability of sourcing and processing fish scales to generate FSB should include harvesting high amounts of scales from these factories, which would provide fish production with added value, and their transference to a GMP facility where scales should be preconditioned and processed as new products for regenerative purposes, fulfilling current regulations in advanced therapies medicinal products [78]. Regarding batch-to-batch variability, further research is necessary to homogenize the production methods and to select specific types of scales. Variability among batches is one of the main problems of bioengineered tissues generated in GMP facilities for clinical use [79], and this is one of the reasons involved in the consideration of these therapies as personalized medicines [80].

This study has some limitations. On the one hand, we evaluated four very common species of fish, but it is obvious that many other species of fish could still be analyzed as sources of FSB. On the other hand, the C-FSB fabricated here contain epithelial cells on their surface, but are devoid of stromal cells within the biomaterial. Although some reports

demonstrated that corneal substitutes and biomaterials without stromal cells could also have clinical usefulness [81], it is clear that culturing stromal cells within the biomaterial layers could increment the potential effectiveness of these products in patients affected by significant corneal stromal damage. In addition, some of our results, particularly those concerning the biomechanical characterization of the different types of FSB exhibit considerable variability and large standard deviations, suggesting that results should be interpreted with caution. Furthermore, in vivo studies should be carried out to compare the novel FSB described here with other previously developed biomaterials such as the NANO-ULCOR bioengineered cornea [31]. Finally, we carried out a preliminary evaluation of the novel products generated by tissue engineering. However, additional research are in need to determine the real clinical potential of these products in clinical trials performed in patients with corneal diseases with the authorization of the Medicines Agencies, as requested for advanced therapies medicinal products [9].

In summary, in this study, we developed and characterized in culture and in laboratory animals several types of FSB as biomaterials with potential usefulness in cornea repair and engineering. Our results demonstrated that these products are highly biocompatible and support corneal cell attachment and differentiation, with good biomechanical and optical properties. This synergy of biological and physical properties supports the use of FSB as a novel promising, sustainable alternative to synthetic materials used in cornea tissue engineering. Of the four types of FSB evaluated here, biomaterials obtained from CC show the most promising results. Clinical trials are needed to determine the effectiveness of these products in patients with severe corneal damage.

#### 5. Institutional review board statement

The study was conducted in accordance with the Declaration of Helsinki and approved by the Institutional Ethics Committee (Comité Coordinador de Ética de la Investigación Biomédica de Andalucía - CCEIBA-), ref. 1915-N-20 (31 March 2023) and 2049-N-23 (8 February 2024). Animal studies were performed in accordance with the guidelines and regulations of the Association for Research in Vision and Ophthalmology (ARVO) for the use of animals in ophthalmic and vision research, following the ARRIVE guidelines (Animal Research: Reporting of In Vivo Experiments) and recommendations for the full and transparent reporting of research involving animals. Animal experimentation was carried out carried out in accordance with the EU Directive 2010/63/EU for animal experiments, and was approved by the regional research and ethics committee for animal experimentation (CEEA) of Consejería de Agricultura, Pesca, Agua y Desarrollo Rural (Junta de Andalucía, Spain), ref. 16/12/2020/147 (17 December 2020) and 14/01/2025/002 (15 January 2025).

#### CRediT authorship contribution statement

I. Garzón: Writing – original draft, Supervision, Investigation, Formal analysis, Conceptualization. J. Muñoz-Hurtado: Validation, Methodology, Investigation, Formal analysis, Data curation. J. Pereira-Martínez: Validation, Methodology, Investigation, Formal analysis, Data curation. C. González-Gallardo: Resources, Project administration, Investigation. A.M. Ionescu: Resources, Methodology, Investigation, Formal analysis. J.C. Cardona: Resources, Methodology, Investigation, Formal analysis. M. Tejada-Casado: Resources, Methodology, Investigation, Formal analysis. M.M. Pérez: Validation, Supervision, Resources. J. Chato-Astrain: Writing – original draft, Supervision, Investigation, Formal analysis, Conceptualization. M. Alaminos: Writing – review & editing, Writing – original draft, Supervision, Project administration, Formal analysis, Conceptualization.

#### Declaration of competing interest

The authors declare that they have no known competing financial

interests or personal relationships that could have appeared to influence the work reported in this paper.

#### Acknowledgement

This paper is dedicated to the memory of Amalia de la Rosa, for her contribution and collaboration with the *in vivo* experiments carried out at the animal facility of the research institute ibs.GRANADA. This research was funded by Instituto de Salud Carlos III (ISCIII), Ministry of Science, Innovation and Universities, grants FIS PI23/00335, FIS PI20/00317 and ICI21/00010 (NANOULCOR). Cofinanced by the European Regional Development Fund (ERDF) through the "Una manera de hacer Europa" program.

#### Appendix A. Supplementary data

Supplementary data to this article can be found online at https://doi.org/10.1016/j.matdes.2025.114703.

#### Data availability

The original data presented in the study are openly available in Zenodo at https://doi.org/10.5281/zenodo.15068771

#### References

- A.K. Raut, S. Mohapatra, G. SiddiquI, S.K. Rajak, R. Sonar, S. Basu, V. Joshi, V. Singh, The human cornea: unraveling its structural chemical, and biochemical complexities, Chem. Biodivers. (2024) e202402224, https://doi.org/10.1002/ cbdv.202402224.
- [2] A. Kumar, H. Yun, M.L. Funderburgh, Y. Du, Regenerative therapy for the Cornea, Prog. Retin. Eye Res. 87 (2022) 101011, https://doi.org/10.1016/j. preteyeres.2021.101011.
- [3] P.M. Mathews, K. Lindsley, A.J. Aldave, E.K. Akpek, Etiology of global corneal blindness and current practices of corneal transplantation: a focused review, Cornea 37 (2018) 1198–1203, https://doi.org/10.1097/ICO.00000000000001666.
- [4] F. Da Silva, J.M.M. Linhares, M. Lira, What intrinsic factors affect the central corneal thickness? Ophthalmic Physiol. Opt. 45 (2025) 315–332, https://doi.org/ 10.1111/opo.13414.
- [5] R. Natarajan, D. Giridhar, Corneal scarring after epithelium-off collagen cross-linking, Indian J. Ophthalmol. 73 (2025) 28–34, https://doi.org/10.4103/IJO.IJO.95\_24.
- [6] S.E. Park, M. Tseng, J.K. Lee, Effectiveness of intracorneal ring segments for keratoconus, Curr. Opin. Ophthalmol. 30 (2019) 220–228, https://doi.org/ 10.1097/ICU.00000000000000582.
- [7] D.T.H. Tan, J.K.G. Dart, E.J. Holland, S. Kinoshita, Corneal transplantation, Lancet 379 (2012) 1749–1761, https://doi.org/10.1016/S0140-6736(12)60437-1.
- [8] R. Al Monla, V. Daien, F. Michon, Advanced bioengineering strategies broaden the therapeutic landscape for corneal failure, Front. Bioeng. Biotechnol. 12 (2024) 1480772, https://doi.org/10.3389/fbioe.2024.1480772.
- [9] C. González-Gallardo, J. Martínez-Atienza, B. Mataix, J.I. Muñoz-Ávila, J. Daniel Martínez-Rodríguez, S. Medialdea, A. Ruiz-García, A. Lizana-Moreno, S. Arias-Santiago, M. de la Rosa-Fraile, I. Garzon, A. Campos, N. Cuende, M. Alaminos, M. González-Andrades, R. Mata, Successful restoration of corneal surface integrity with a tissue-engineered allogeneic implant in severe keratitis patients, Biomed. Pharmacother. 162 (2023) 114612, https://doi.org/10.1016/j. hispho. 2023.114613.
- [10] Z. Chen, J. You, X. Liu, S. Cooper, C. Hodge, G. Sutton, J.M. Crook, G.G. Wallace, Biomaterials for corneal bioengineering, Biomed. Mater. 13 (2018) 032002, https://doi.org/10.1088/1748-605X/aa92d2.
- [11] A. Isaacson, S. Swioklo, C.J. Connon, 3D bioprinting of a corneal stroma equivalent, Exp. Eye Res. 173 (2018) 188–193, https://doi.org/10.1016/j. exer.2018.05.010.
- [12] B. Kong, Y. Chen, R. Liu, X. Liu, C. Liu, Z. Shao, L. Xiong, X. Liu, W. Sun, S. Mi, Fiber reinforced GelMA hydrogel to induce the regeneration of corneal stroma, Nat. Commun. 11 (2020) 1435, https://doi.org/10.1038/s41467-020-14887-9.
- [13] S.S. Mahdavi, M.J. Abdekhodaie, S. Mashayekhan, A. Baradaran-Rafii, A. R. Djalilian, Bioengineering approaches for corneal regenerative medicine, Tissue Eng. Regen. Med. 17 (2020) 567–593, https://doi.org/10.1007/s13770-020-00262-8.
- [14] C.-J. Yang, D.D. Nguyen, J.-Y. Lai, Poly(I-Histidine)-mediated on-demand therapeutic delivery of roughened ceria nanocages for treatment of chemical eye injury, Adv. Sci. (Weinh) 10 (2023) e2302174, https://doi.org/10.1002/ advs.202302174
- [15] D.D. Nguyen, C.-H. Yao, L.-J. Luo, H.-C. Chen, Y.-J. Hsueh, D.-H.-K. Ma, J.-Y. Lai, Oxidation-mediated scaffold engineering of hyaluronic acid-based microcarriers enhances corneal stromal regeneration, Carbohydr. Polym. 292 (2022) 119668, https://doi.org/10.1016/j.carbpol.2022.119668.

- [16] T.-Y. Ger, C.-J. Yang, S. Ghosh, J.-Y. Lai, Biofunctionalization of nanoceria with sperminated hyaluronan enhances drug delivery performance for corneal alkali burn therapy, Chem. Eng. J. 476 (2023) 146864, https://doi.org/10.1016/j. cei 2023 146864
- [17] W.-L. Wang, Y.-H. Lai, C.-H. Huang, J.-Y. Lai, C.-H. Yao, Lumbrokinase-containing gelatin nanofibers with multiple bioactivities for effective skin wound healing, Mater. Today Bio 32 (2025) 101713, https://doi.org/10.1016/j. mtbio.2025.101713.
- [18] J.L. Vidal, T. Jin, E. Lam, F. Kerton, A. Moores, Blue is the new green: valorization of crustacean waste, Curr. Res. Green Sustainable Chem. 5 (2022) 100330, https://doi.org/10.1016/j.crgsc.2022.100330.
- [19] L. Salvatore, N. Gallo, M.L. Natali, L. Campa, P. Lunetti, M. Madaghiele, F.S. Blasi, A. Corallo, L. Capobianco, A. Sannino, Marine collagen and its derivatives: versatile and sustainable bio-resources for healthcare, Mater. Sci. Eng. C Mater. Biol. Appl. 113 (2020) 110963, https://doi.org/10.1016/j.msec.2020.110963.
- [20] O. Ortiz-Arrabal, R. Carmona, Ó.-D. García-García, J. Chato-Astrain, D. Sánchez-Porras, A. Domezain, R.-I. Oruezabal, V. Carriel, A. Campos, M. Alaminos, Generation and evaluation of novel biomaterials based on decellularized sturgeon cartilage for use in tissue engineering, Biomedicines 9 (2021) 775, https://doi.org/10.3390/biomedicines9070775.
- [21] W. Yang, I.H. Chen, B. Gludovatz, E.A. Zimmermann, R.O. Ritchie, M.A. Meyers, Natural flexible dermal armor, Adv. Mater. 25 (2013) 31–48, https://doi.org/ 10.1002/adma.201202713.
- [22] Y.-J. Hsueh, D.-H.-K. Ma, K.-S.-C. Ma, T.-K. Wang, C.-H. Chou, C.-C. Lin, M.-C. Huang, L.-J. Luo, J.-Y. Lai, H.-C. Chen, Extracellular matrix protein coating of processed fish scales improves human corneal endothelial cell adhesion and proliferation, Transl. Vis. Sci. Technol. 8 (2019) 27, https://doi.org/10.1167/tvst.8.3.27.
- [23] S. Matthyssen, B. Van den Bogerd, S.N. Dhubhghaill, C. Koppen, N. Zakaria, Corneal regeneration: a review of stromal replacements, Acta Biomater. 69 (2018) 31–41, https://doi.org/10.1016/j.actbio.2018.01.023.
- [24] S. Chen, N. Hirota, M. Okuda, M. Takeguchi, H. Kobayashi, N. Hanagata, T. Ikoma, Microstructures and rheological properties of tilapia fish-scale collagen hydrogels with aligned fibrils fabricated under magnetic fields, Acta Biomater. 7 (2011) 644–652, https://doi.org/10.1016/j.actbio.2010.09.014.
- [25] K. Tjoa, M.H. Nadhif, S.S. Utami, S.R. Kusuma, P.Y. Astagiri, G.A. Adriono, Mechanical, optical, chemical, and biological evaluations of fish scale-derived scaffold for corneal replacements: a systematic review, Int. J. Biol. Macromol. 267 (2024) 131183, https://doi.org/10.1016/j.ijbiomac.2024.131183.
- [26] S. Krishnan, S. Sekar, M.F. Katheem, S. Krishnakumar, T.P. Sastry, Fish scale collagen—a novel material for corneal tissue engineering, Artif. Organs 36 (2012) 829–835, https://doi.org/10.1111/j.1525-1594.2012.01452.x.
- [27] S.A. Prahl, M.J. van Gemert, A.J. Welch, Determining the optical properties of turbid mediaby using the adding-doubling method, Appl. Opt. 32 (1993) 559–568, https://doi.org/10.1364/AO.32.000559.
- [28] G. Cheng, L. Chen, H. Feng, B. Jiang, Y. Ding, Preliminary study on fish scale collagen lamellar matrix as artificial cornea, Membranes (Basel) 11 (2021) 737, https://doi.org/10.3390/membranes11100737.
- [29] I. Garzón, J. Muñoz-Hurtado, J. Pereira-Martínez, A.M. Ionescu, J. de la C. Cardona, M. Tejada-Casado, M.D.M. Pérez, F. Campos, J. Chato-Astrain, M. Alaminos, Development of Novel Squid Gladius Biomaterials for Cornea Tissue Engineering, Mar Drugs 22 (2024) 535. https://doi.org/10.3390/md22120535.
- [30] C.-A. Alfonso-Rodríguez, I. Garzón, J. Garrido-Gómez, A.-C.-X. Oliveira, M.-Á. Martín-Piedra, G. Scionti, V. Carriel, P. Hernández-Cortés, A. Campos, M. Alaminos, Identification of histological patterns in clinically affected and unaffected palm regions in dupuytren's disease, PLoS One 9 (2014) e112457, https://doi.org/10.1371/journal.pone.0112457.
- [31] O. Ortiz-Arrabal, C. Blanco-Elices, C. González-Gallardo, D. Sánchez-Porras, M. Etayo-Escanilla, P.Á. Fernández, J. Chato-Astrain, Ó.-D. García-García, I. Garzón, M. Alaminos, Histological, histochemical, and immunohistochemical characterization of NANOULCOR nanostructured fibrin-agarose human cornea substitutes generated by tissue engineering, BMC Med. 22 (2024) 531, https://doi. org/10.1186/s12916-024-03759-4.
- [32] C.A. Schneider, W.S. Rasband, K.W. Eliceiri, NIH image to ImageJ: 25 years of image analysis, Nat. Methods 9 (2012) 671–675, https://doi.org/10.1038/ nmeth.2089.
- [33] J. Hernández-Andrés, J. Romero, R.L. Lee, Colorimetric and spectroradiometric characteristics of narrow-field-of-view clear skylight in Granada, Spain, J. Opt. Soc. Am. A Opt. Image Sci. Vis. 18 (2001) 412–420, https://doi.org/10.1364/ josaa.18.000412.
- [34] F.H. Imai, M.R. Rosen, R.S. Berns, M.R. Rosen, R.S. Berns, Comparative Study of Metrics for Spectral Match Quality, Conference on Colour in Graphics, Imaging, and Vision 1 (2002) 492–496. https://doi.org/10.2352/CGIV.2002.1.1.art00103.
- [35] X. Ning, R. Wang, N. Liu, Y. You, Y. Wang, J. Wang, Y. Wang, Z. Chen, H. Zhao, T. Wu, Three-dimensional structured PLCL/ADM bioactive aerogel for rapid repair of full-thickness skin defects, Biomater. Sci. 12 (2024) 6325–6337, https://doi.org/ 10.1039/d4bm01214c.
- [36] T.H. van Essen, L. van Zijl, T. Possemiers, A.A. Mulder, S.J. Zwart, C.-H. Chou, C. C. Lin, H.J. Lai, G.P.M. Luyten, M.J. Tassignon, N. Zakaria, A. El Ghalbzouri, M. J. Jager, Biocompatibility of a fish scale-derived artificial cornea: Cytotoxicity, cellular adhesion and phenotype, and in vivo immunogenicity, Biomaterials 81 (2016) 36–45, https://doi.org/10.1016/j.biomaterials.2015.11.015.
- [37] C.C. Lin, R. Ritch, S.M. Lin, M.-H. Ni, Y.-C. Chang, Y.L. Lu, H.J. Lai, F.-H. Lin, A new fish scale-derived scaffold for corneal regeneration, Eur. Cell. Mater. 19 (2010) 50–57.

- [38] T.H. van Essen, C.C. Lin, A.K. Hussain, S. Maas, H.J. Lai, H. Linnartz, T.J.T.P. van den Berg, D.C.F. Salvatori, G.P.M. Luyten, M.J. Jager, A fish scale-derived collagen matrix as artificial cornea in rats: properties and potential, Invest. Ophthalmol. Vis. Sci. 54 (2013) 3224–3233, https://doi.org/10.1167/iovs.13-11799.
- [39] W.S. Leibel, Antisera probes to an atypical pseudocholinesterase from surgeonfish reveal immunochemical variability and tissue-specific molecular polymorphism, J. Exp. Zool. 247 (1988) 209–223, https://doi.org/10.1002/jez.1402470304.
- [40] P.N.T. Wells, H.-D. Liang, Medical ultrasound: imaging of soft tissue strain and elasticity, J. R. Soc. Interface 8 (2011) 1521–1549, https://doi.org/10.1098/ rsif.2011.0054.
- [41] E. Hammelef, C.J. Rapuano, D.A. Benedetto, Z.A. Syed, J.S. Myers, M. R. Razeghinejad, F.H. Silver, J.S. Pulido, New forays into measurement of ocular biomechanics, Curr. Opin. Ophthalmol. 35 (2024) 225, https://doi.org/10.1097/ ICII.000000000001032.
- [42] G. Greco, H. Mirbaha, B. Schmuck, A. Rising, N.M. Pugno, Artificial and natural silk materials have high mechanical property variability regardless of sample size, Sci. Rep. 12 (2022) 3507, https://doi.org/10.1038/s41598-022-07212-5.
- [43] Y. Hashimoto, J. Negishi, S. Funamoto, T. Kimura, H. Kobayashi, T. Oshika, A. Kishida, Preparation, physico-biochemical characterization, and proteomic analysis of highly transparent corneal extracellular matrices for lamellar keratoplasty and tissue-engineered cornea construction, Mater. Today Bio 28 (2024) 101241, https://doi.org/10.1016/j.mtbio.2024.101241.
- [44] R.D. Peters, S.D. Noble, Characterization of leaf surface phenotypes based on light interaction, Plant Methods 19 (2023) 26, https://doi.org/10.1186/s13007-023-01004-2
- [45] L. Britz, M. Hammer, G. Labuz, A. Zielinska, F. Jester, J. Freudenberg, U. Bunz, C. Scholz, G.U. Auffarth, T.M. Yildirim, Impact of calcium and phosphorus levels on optical deterioration in primary and secondary intraocular lens calcification, Transl. Vis. Sci. Technol. 13 (2024) 18, https://doi.org/10.1167/tvst.13.10.18.
- [46] F. Muñoz, Z.S. Haidar, A. Puigdollers, I. Guerra, M.C. Padilla, N. Ortega, M. Balcells, M.J. García, Efficient hydroxyapatite extraction from salmon bone waste: an improved lab-scaled physico-chemico-biological process, Molecules 29 (2024) 4002, https://doi.org/10.3390/molecules29174002.
- [47] C.-S. Wu, D.-Y. Wu, S.-S. Wang, Biodegradable composite nanofiber containing fish-scale extracts, ACS Appl. Bio Mater. 4 (2021) 462–469, https://doi.org/ 10.1021/acsabm.0c00955.
- [48] W. Pon-On, P. Suntornsaratoon, N. Charoenphandhu, J. Thongbunchoo, N. Krishnamra, I.M. Tang, Hydroxyapatite from fish scale for potential use as bone scaffold or regenerative material, Mater. Sci.. Eng. C Mater. Biol. Appl. 62 (2016) 183–189, https://doi.org/10.1016/j.msec.2016.01.051.
- [49] S.C. Mkhize, S.C. Onwubu, T.H. Mokhothu, P.S. Mdluli, A.K. Mishra, Comparative assessment of the remineralization characteristics of nano-hydroxyapatite extracted from fish scales and eggshells, J. Appl. Biomater. Funct. Mater. 21 (2023) 22808000231180390, https://doi.org/10.1177/22808000231180390.
- [50] M. Prakasam, J. Locs, K. Salma-Ancane, D. Loca, A. Largeteau, L. Berzina-Cimdina, Fabrication properties and applications of dense hydroxyapatite: A review, J. Funct. Biomater. 6 (2015) 1099–1140, https://doi.org/10.3390/jfb6041099.
- [51] C.H.C. Keck, E.L. Schmidt, R.H. Roth, B.M. Floyd, A.P. Tsai, H.B. Garcia, M. Cui, X. Chen, C. Wang, A. Park, S. Zhao, P.A. Liao, K.M. Casey, W. Reineking, S. Cai, L.-Y. Zhang, Q. Yang, L. Yuan, A. Baghdasaryan, E.R. Lopez, L. Cooper, H. Cui, D. Esquivel, K. Brinson, X. Chen, T. Wyss-Coray, T.P. Coleman, M.L. Brongersma, C.R. Bertozzi, G.X. Wang, J.B. Ding, G. Hong, Color-neutral and reversible tissue transparency enables longitudinal deep-tissue imaging in live mice, bioRxiv (2025) 2025.02.20.639185. https://doi.org/10.1101/2025.02.20.639185.
- [52] L.X. Yu, Pharmaceutical quality by design: product and process development, understanding, and control, Pharm. Res. 25 (2008) 781–791, https://doi.org/ 10.1007/s11095-007-9511-1.
- [53] O. Ortiz Arrabal, E. Bullejos Martínez, J. Chato Astrain, V. Carriel Araya, A. Martínez Plaza, M.Á. Martín Piedra, I.J. Garzón Bello, R. Fernández Valadés, A. España López, I.A. Rodríguez, M. Alaminos, Evaluation of holothurian ossicles as a biological biomaterial for mandibular bone regeneration, (2025). https://doi.org/10.22203/eCM.v049a01.
- [54] L. Rico-Sánchez, I. Garzón, M. González-Andrades, A. Ruíz-García, M. Punzano, A. Lizana-Moreno, J.I. Muñoz-Ávila, M.D.C. Sánchez-Quevedo, J. Martínez-Atienza, L. Lopez-Navas, R. Sanchez-Pernaute, R.I. Oruezabal, S. Medialdea, M.D. C. Gonzalez-Gallardo, G. Carmona, S. Sanbonmatsu-Gámez, M. Perez, P. Jimenez, N. Cuende, A. Campos, M. Alaminos, Successful development and clinical translation of a novel anterior lamellar artificial cornea, J. Tissue Eng. Regen. Med. 13 (2019) 2142–2154, https://doi.org/10.1002/term.2951.
  [55] C.R. Harrell, Therapeutic potential of d-MAPPS<sup>TM</sup> for ocular inflammatory diseases
- [55] C.R. Harrell, Therapeutic potential of d-MAPPS<sup>111</sup> for ocular inflammatory diseases and regeneration of injured corneal and retinal tissue, Int. J. Mol. Sci. 23 (2022) 13528, https://doi.org/10.3390/ijms232113528.
- [56] K. Yamamoto, K. Igawa, K. Sugimoto, Y. Yoshizawa, K. Yanagiguchi, T. Ikeda, S. Yamada, Y. Hayashi, Biological safety of fish (tilapia) collagen, Biomed Res. Int. 2014 (2014) 630757, https://doi.org/10.1155/2014/630757.
- [57] H. Sugiura, S. Yunoki, E. Kondo, T. Ikoma, J. Tanaka, K. Yasuda, In vivo biological responses and bioresorption of tilapia scale collagen as a potential biomaterial, J. Biomater. Sci. Polym. Ed. 20 (2009) 1353–1368, https://doi.org/10.1163/ 092050609X12457418396658.
- [58] Y. Zhou, Y. Chai, K. Mikami, M. Tagaya, Biomimetic mineralization in external layer of decalcified fish scale, Biomimetics (Basel) 7 (2022) 97, https://doi.org/ 10.3390/biomimetics7030097.
- [59] H. Toshida, T. Kasahara, M. Kiriyama, Y. Iwasaki, J. Sugita, K. Ichikawa, T. Ohta, K. Miyahara, Early clinical outcomes of the first commercialized human autologous ex vivo cultivated oral mucosal epithelial cell transplantation for limbal stem cell

- deficiency: two case reports and literature review, Int. J. Mol. Sci. 24 (2023) 8926, https://doi.org/10.3390/jims24108926.
- [60] I. Garzón, J. Chato-Astrain, C. González-Gallardo, A. Ionescu, J. de la C. Cardona, M. Mateu, C. Carda, M.D.M. Pérez, M.Á. Martín-Piedra, M. Alaminos, Long-Term in vivo Evaluation of Orthotypical and Heterotypical Bioengineered Human Corneas, Front Bioeng Biotechnol 8 (2020) 681. https://doi.org/10.3389/fbioe.2020.00681.
- [61] K. Kolind, K.W. Leong, F. Besenbacher, M. Foss, Guidance of stem cell fate on 2D patterned surfaces, Biomaterials 33 (2012) 6626–6633, https://doi.org/10.1016/j.biomaterials.2012.05.070.
- [62] P.A. Janmey, D.A. Fletcher, C.A. Reinhart-King, Stiffness sensing by cells, Physiol. Rev. 100 (2020) 695–724, https://doi.org/10.1152/physrev.00013.2019.
- [63] Q. Zhang, X. Zhou, W. Zhang, X. Wang, S. Dou, L. Zhao, R. El-Habta, Q. Zhou, L. J. Backman, P. Danielson, Corneal strain influences keratocyte proliferation and migration through upregulation of ALDH3A1 expression, FASEB J. 38 (2024) e70236. https://doi.org/10.1096/fj.202401392R.
- [64] J. Baek, K.I. Lee, H.J. Ra, M.K. Lotz, D.D. D'Lima, Collagen fibrous scaffolds for sustained delivery of growth factors for meniscal tissue engineering, Nanomedicine (Lond.) 17 (2022) 77–93, https://doi.org/10.2217/nnm-2021-0313.
- [65] M.A. Martin-Piedra, G. Carmona, F. Campos, V. Carriel, A. Fernández-González, A. Campos, N. Cuende, I. Garzón, P. Gacto, M. Alaminos, Histological assessment of nanostructured fibrin-agarose skin substitutes grafted in burnt patients A timecourse study, Bioeng. Transl. Med. 8 (2023) e10572, https://doi.org/10.1002/ btm2.10572.
- [66] B. Bánó, A. Bolotovskiy, B. Levin, G.M.T. Mattox, M. Cetra, I. Czeglédi, P. Takács, Scale morphology is a promising, additional tool for exploring the taxonomy and ecology of freshwater fishes, Fish Fish. 25 (2024) 569–588, https://doi.org/ 10.1111/faf.12826.
- [67] A. Marino Cugno Garrano, G. La Rosa, D. Zhang, L.N. Niu, F.R. Tay, H. Majd, D. Arola, On the mechanical behavior of scales from Cyprinus carpio, J. Mech. Behav. Biomed. Mater. 7 (2012) 17–29, https://doi.org/10.1016/j. jmbbm.2011.07.017.
- [68] H. Quan, W. Yang, M. Lapeyriere, E. Schaible, R.O. Ritchie, M.A. Meyers, Structure and mechanical adaptability of a modern elasmoid fish scale from the common carp, Matter 3 (2020) 842–863, https://doi.org/10.1016/j.matt.2020.05.011.
- [69] J.W. Ruberti, A. Sinha Roy, C.J. Roberts, Corneal biomechanics and biomaterials, Annu. Rev. Biomed. Eng. 13 (2011) 269–295, https://doi.org/10.1146/annurev-bioeng-070909-105243.
- [70] K.Y.H. Chee, A. Kicic, S.J. Wiffen, Limbal stem cells: the search for a marker, Clin. Exp. Ophthalmol. 34 (2006) 64–73, https://doi.org/10.1111/j.1442-9071.2006.01147.x.
- [71] R. Sharif, B. Fowler, D. Karamichos, Collagen cross-linking impact on keratoconus extracellular matrix, PLoS One 13 (2018) e0200704, https://doi.org/10.1371/ journal.pone.0200704.
- [72] E. Maguen, Y.S. Rabinowitz, L. Regev, M. Saghizadeh, T. Sasaki, A.V. Ljubimov, Alterations of extracellular matrix components and proteinases in human corneal buttons with INTACS for post-laser in situ keratomileusis keratectasia and keratoconus, Cornea 27 (2008) 565–573, https://doi.org/10.1097/ ICO.0b013e318165b1cd.
- [73] H. Li, R. Chen, Z. Jia, C. Wang, Y. Xu, C. Li, H. Xia, D. Meng, Porous fish collagen for cartilage tissue engineering, Am. J. Transl. Res. 12 (2020) 6107–6121.
- [74] C. Shaw, K. Knopf, W. Kloas, Fish feeds in aquaponics and beyond: a novel concept to evaluate protein sources in diets for circular multitrophic food production systems, Sustainability 14 (2022) 4064, https://doi.org/10.3390/su14074064.
- [75] X. Liu, Q. Hu, Y. Shen, Y. Wu, L. Gao, X. Xu, G. Hao, Research progress on antioxidant peptides from fish by-products: purificationidentification, and structure-activity relationship, Metabolites 14 (2024) 561, https://doi.org/ 10.3390/metabol4100561.
- [76] H. Agnieray, J.L. Glasson, Q. Chen, M. Kaur, L.J. Domigan, Recent developments in sustainably sourced protein-based biomaterials, Biochem. Soc. Trans. 49 (2021) 953–964, https://doi.org/10.1042/BST20200896.
- [77] J. Ohlberger, E.J. Ward, R.E. Brenner, M.E. Hunsicker, S.B. Haught, D. Finnoff, M. A. Litzow, T. Schwoerer, G.T. Ruggerone, C. Hauri, Non-stationary and interactive effects of climate and competition on pink salmon productivity, Glob. Chang. Biol. 28 (2022) 2026–2040, https://doi.org/10.1111/gcb.16049.
- [78] K.F. Pearce, M. Hildebrandt, H. Greinix, S. Scheding, U. Koehl, N. Worel, J. Apperley, M. Edinger, A. Hauser, E. Mischak-Weissinger, A.M. Dickinson, M. W. Lowdell, Regulation of advanced therapy medicinal products in Europe and the role of academia, Cytotherapy 16 (2014) 289–297, https://doi.org/10.1016/j. jcyt.2013.08.003.
- [79] M. Kropp, N. Harmening, T. Bascuas, S. Johnen, E. De Clerck, V. Fernández, M. Ronchetti, R. Cadossi, C. Zanini, D. Scherman, Z. Ivics, C. Marie, Z. Izsvák, G. Thumann, GMP-grade manufacturing and quality control of a non-virally engineered advanced therapy medicinal product for personalized treatment of agerelated macular degeneration, Biomedicines 10 (2022) 2777, https://doi.org/10.3390/biomedicines10112777.
- [80] F.A. Kakroodi, E. Khodadoust, M. Alizadeh, R.S. Hayaei Tehrani, P.A. Sarabi, M. Rahmanian, M. Vosough, Current challenges and future directions of ATMPs in regenerative medicine, Regen. Ther. 30 (2025) 358–370, https://doi.org/10.1016/ j.reth.2025.06.017.
- [81] C.-M. Liang, D.-J. Hsieh, F.-W. Tseng, P. Srinivasan, M.-L. Yeh, M.-C. Tai, Acellular porcine cornea produced by supercritical carbon dioxide extraction: a potential substitute for human corneal regeneration, Cornea 41 (2022) 328–338, https://doi. org/10.1097/ICO.0000000000002790.